CHAPTER 4: III-V COMPOUND SEMICONDUCTORS

Till date there have been many studies on the structural and electronic properties of group III-V compound semiconductors. The detailed literatures available on these semiconductors have been discussed in chapter 1 (Introduction), sub section 1.2 (Review of literatures). But the high-pressure study on the electronic structures and elastic properties is still very rare. The experimental study of these quantities at high pressure is very difficult and therefore, many theoretical calculations are usually used.The main aim of the study in the present chapter is to have a detailed understanding of the structural, electronic, phase transition as well as the effects of pressure on the electronic and elastic properties of the group III-V compound semiconductors: GaP, GaAs, InP and InAs.

4.1. STRUCTURAL STABILITY AND PHASE TRANSITION

The static equilibrium properties of the crystal structure of zincblende (ZB) and rocksalt (RS) of GaP, GaAs, InP and InAs are obtained by minimization of the total energy with respect to the unit cell volumes per molecule and fitting it to the Birch–Murnaghan equation [81]. The phase with the lowest Gibbs energy at a given pressure and temperature determines the Enthalpy of the phase. Since our calculation is done at zero temperature we have ignored the entropy contribution. Therefore the structural phase transition has been calculated from the condition of equal enthalpies i.e. $H = E + PV$.

The structural properties and Phase transition of III-V compound semiconductors: GaP, GaAs, InP and InAs are discussed in this section. In all calculations, we have used LDA and GGA exchange correlations to see the comparative results.

(a) Gallium Phosphide (GaP)

The total energy as a function of volume of GaP for both the ZB and RS structure that are calculated with LDA and GGA for structure optimization are shown in

figure 4.1. From the figure, it is observed that GaP-ZB structure has lower total energy at the equilibrium volume in both LDA and GGA methods thus indicating that GaP in ZB structure is more stable than the RS structure.

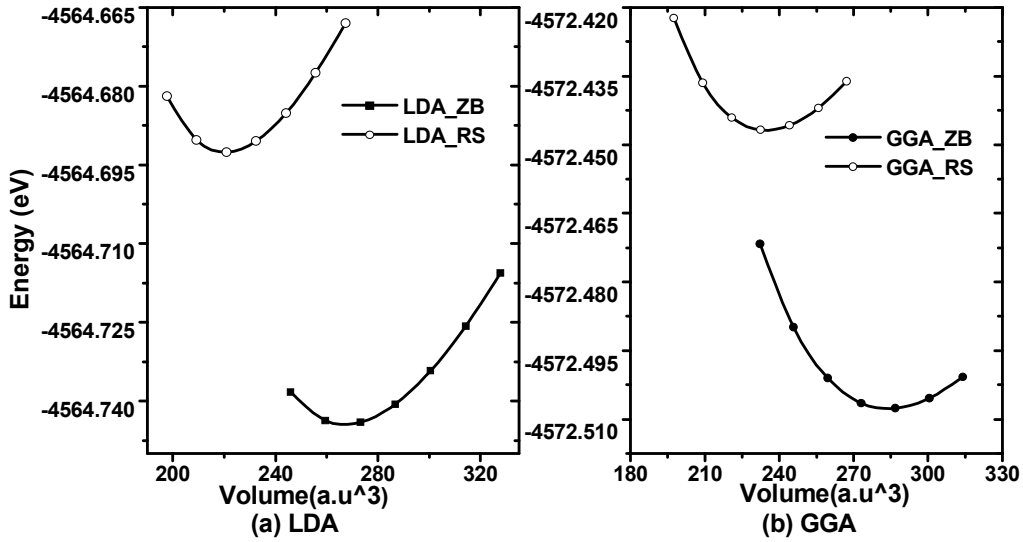

Figure 4.1.Total energy as a function of primitive cell volume of GaP-ZB and GaP-RS with (a) LDA method and (b) GGA method

Table 4.1. Experimental and calculated ground state structural parameters of GaP in ZB and RS structure

		Zinc Blende (ZB) Strucutre			**Rock Salt (RS) Structure**		
		a_0 (A^0)	B_0 (GPa)	$B^/$	a_0 (A^0)	B_0 (GPa)	$B^/$
Present work	LDA	5.41	91.19	4.72	5.07	105.80	4.83
	GGA	5.52	77.71	4.34	5.18	88.34	4.84
Expt. work		5.47[a], 5.50[b], 5.45[c]	77.2[b],	4.88[b],	-	-	-
Other Theo. calculation		5.41[d], 5.54[e], 5.51[f]	90.0[d], 76.0[f],	4.50[d], 4.59[f]	5.165[g], 5.160[f]	87.3[g], 87.59[f]	3.78[g], 4.54[f]

[a]Ref[82], [b]Ref[83], [c]Ref[84], [d]Ref[12], [e]Ref[85] , [f]Ref[13], [g]Ref[86]

The results of present study of GaP-ZB and GaP-RS are compared with other available experimental and theoretical data and are given in table 4.1. For the GaP-ZB phase for which the experimental values are available for comparison, the lattice parameter calculated with LDA method shows a difference of only 0.9% while that of GGA shows a difference of 0.36% which is quite acceptable under the 2% difference. Thus our results are in good agreement with other studies and used for further calculation of phase transition and energy band structure.

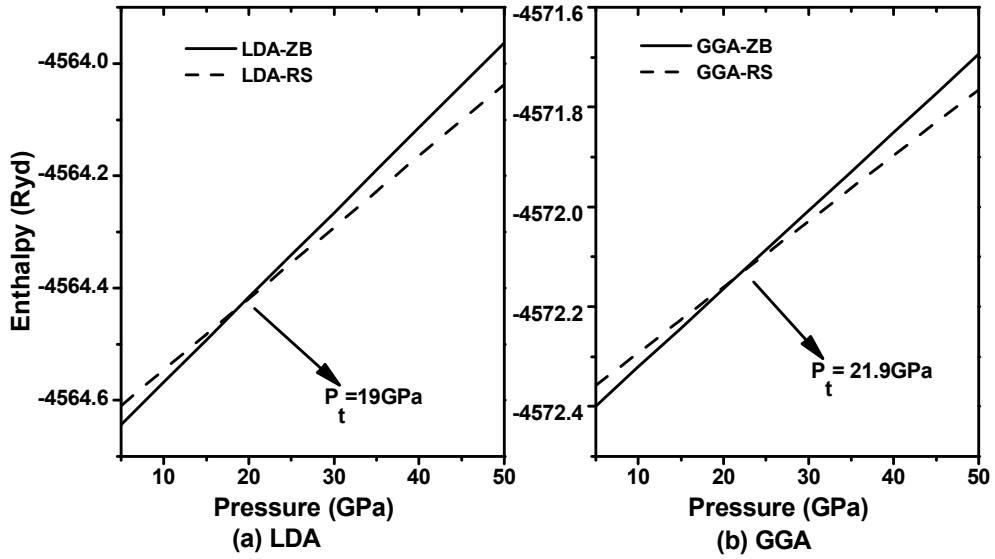

Figure 4.2. Enthalpy as a function of pressure for ZB and RS phase of GaP within (a) LDA method and (b) GGA method

Table 4.2. Phase transition pressure 'P_t(GPa)' and volume collapse of GaP

	Present calculation	**Expt. results**	**Theoretical results**
Transition pressure (P_t)(GPa)	19 (LDA) 21.9 (GGA)	22[a],24±0.3[b], 21.5±0.8 [c]	21.7[d], 18.8[e], 16.8[f],
Volume collapse (%)	14.11		14[g], 16[h]

[a]Ref[87], [b]Ref[88], [c]Ref[89], [d]Ref[90], [e]Ref[91], [f]Ref[92], [g]Ref[93], [h]Ref[94]

Under the induced pressure, GaP in ZB structure transforms to RS structure. When the phase transition takes place, the Enthalpy of both the phases are same. Thus the

pressure at equal Enthalpy determines the phase transition pressure. Figure 4.2 shows the variation of Enthalpy with pressure for both the methods i.e. LDA and GGA. The transition pressure with LDA method shows a phase transition of 19 GPa pressure while within GGA method the phase transformation takes place at 21.9 GPa pressure which is more nearer to experimental result as shown in table 4.2. Since GGA gives us better calculation of the phase transition we have calculated the volume collapse of GaP within the GGA only. The normalised volume as a function of pressure is also shown in figure 4.3. During the phase transition the normalised volume of the ZB and RS phase is 0.829 and 0.688 respectively with a volume decrease of 14.11% indicating that ZB phase is more compressible than the RS phase.

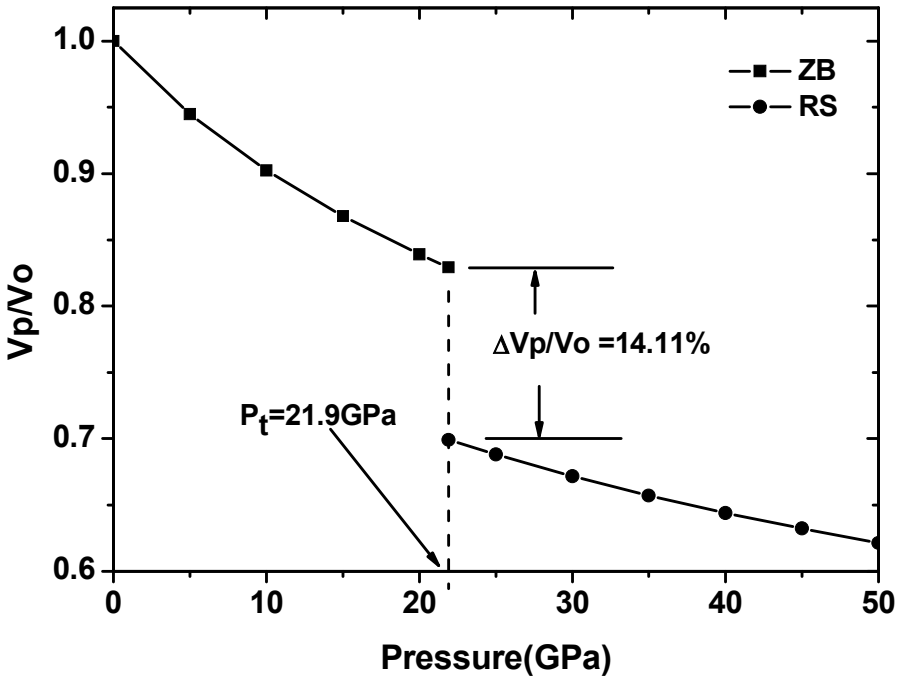

Figure 4.3. Normalized volume as a function of pressure of GaP-ZB and GaP-RS

(b) Gallium Arsenide (GaAs)

The results of structural properties and phase transition of GaAs are discussed in this sub section following the same methods of calculations as before.

In Figure 4.4, the total energy as a function of volume of GaAs shows that the GaAs in ZB structure is more stable than the RS structure. The present calculated parameters are compared with other experimental and theoretical data in table 4.3. The present results are in good agreement with other studies and thus used for phase transition and energy band structure study.

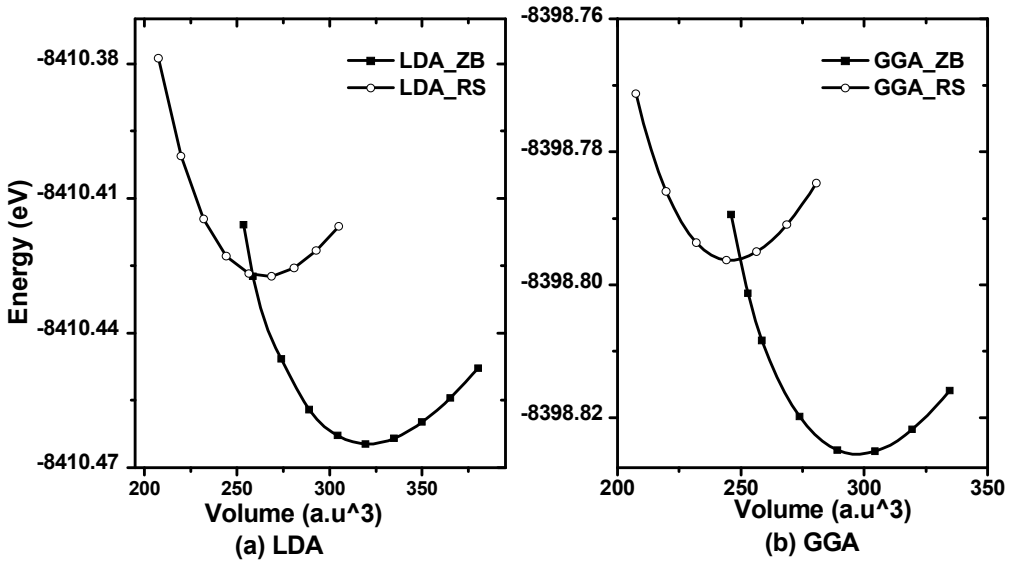

Figure 4.4. Total energy as a function of primitive cell volume for GaAs-ZB and GaAs-RS with (a) LDA method and (b) GGA method

Table 4.3. Experimental and calculated ground state structural parameters of GaAs in ZB and RS structure

		Zinc Blende (ZB) Structure			**Rock Salt (RS) Structure**		
		a_0 (A^0)	B_0 (GPa)	$B^/$	a_0 (A^0)	B_0 (GPa)	$B^/$
Present work	LDA	5.61	75.46	4.93	5.26	88.73	4.95
	GGA	5.74	61.08	4.80	5.37	71.10	4.90
Expt. work		5.65[a]	75.7[b], 74.8[c]	4.00[b], 4.56[c]	-	-	-
Other Theo. calculation		5.74[d], 5.64[e], 5.65[f]	75.76[e], 73.4[f]	4.71[e], 4.50[f]	5.29[e], 5.32[f]	73.54[b], 83.68[e]	5.10[e], 4.77[f]

[a]Ref[95], [b]Ref[96], [c]Ref[97], [d]Ref[98], [e]Ref[99], [f]Ref[100]

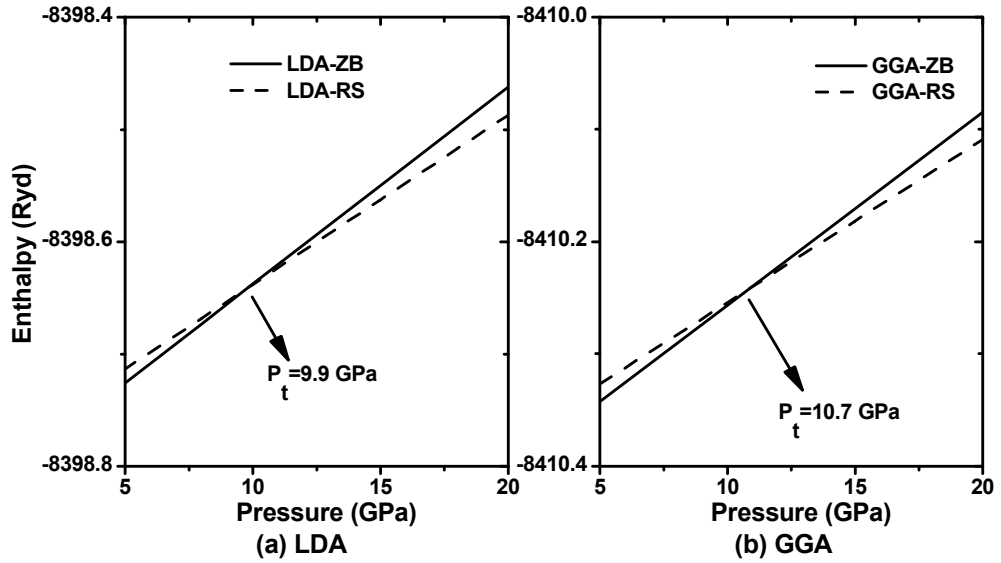

Figure. 4.5. Enthalpy as a function of pressure for ZB and RS phase of GaAs with (a) LDA method and (b) GGA method

Table 4.4. Phase transition pressure 'P_t(GPa)' and volume collapse of GaAs

	Present calculation	**Expt. results**	**Theoretical results**
Transition pressure (P_t)(GPa)	9.9 (LDA) 10.7 (GGA)	12±1.5[a]	12.0[b], 16.3[c], 17.3[d],10.5[e]
Volume collapse (%)	14.2	-	-

[a]Ref[101], [b]Ref[102], [c]Ref[96], [d]Ref[99], [e]Ref[103]

The Enthalpy graph as shown in figure 4.5 shows a transition pressure of 9.9 GPa pressure with LDA method while the transition pressure with GGA method is 10.7 GPa pressure. The normalised volume (with GGA method in figure 4.6) of ZB and RS phase is 0.876 and 0.734 respectively. Thus there is a volume decrease of 14.2% during the phase transition. It concludes that ZB phase is more compressible than the RS phase. The results of phase transition and volume collapse are compared with other experimental and theoretical studies in table 4.4.

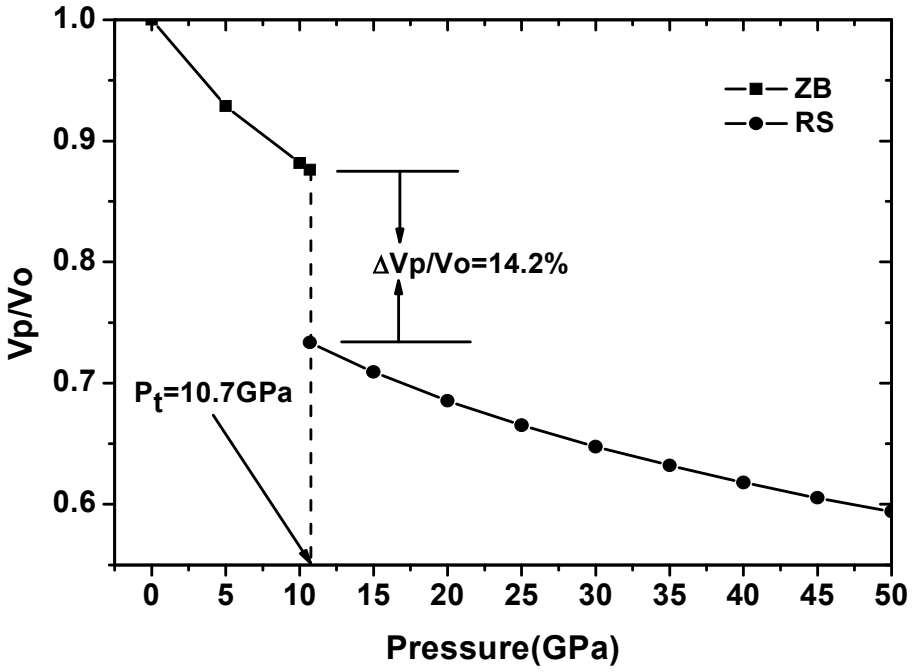

Figure 4.6. Normalized volume as a function of pressure for GsAs-ZB and GaAs-RS

(c) Indium Phosphide (InP)

In this subsection, the structural parameters and phase transition of InP are studied. The total energy as a function of volume of InP are shown in figure 4.7 and the ZB structure of InP is found to be more stable than the RS structure. In table 4.5, the results of present calculated parameters of InP-ZB and InP-RS are compared with other experimental and theoretical data.

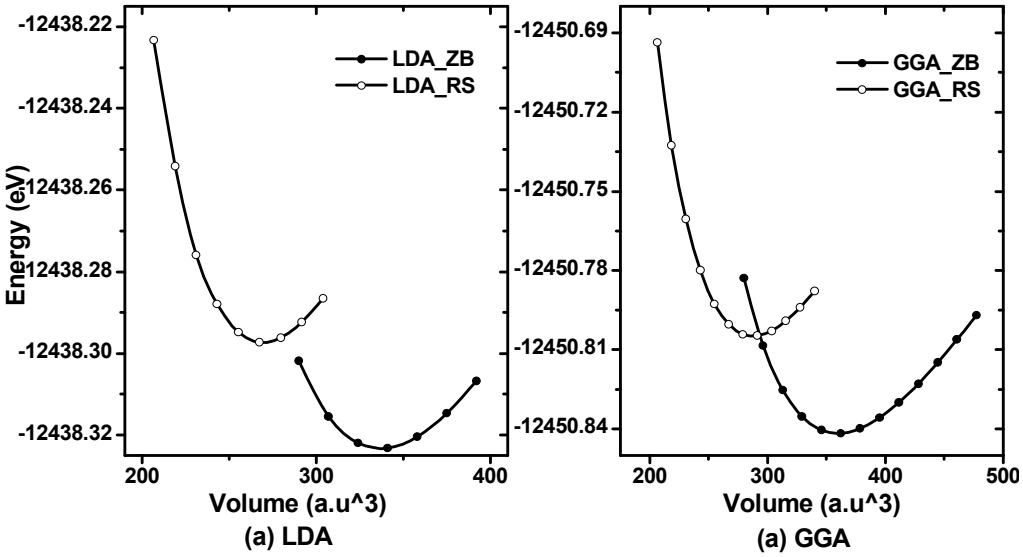

Figure 4.7.Total energy as a function of primitive cell volume for InP-ZB and InP-RS with (a) LDA method and (b) GGA method

Table 4.5. Lattice constant 'a(A^0)', bulk modulus 'B(GPa)' and pressure derivative of bulk modulus ($B^/$) of ZB and RS structure of InP at zero pressure

		Zinc Blende (ZB) Structure			**Rock Salt (RS) Structure**		
		a_0 (A^0)	B_0 (GPa)	$B^/$	a_0 (A^0)	B_0 (GPa)	$B^/$
Present work	LDA	5.84	71.93	4.79	5.42	88.61	5.04
	GGA	5.97	60.5	4.64	5.54	74.78	4.76
Expt. work		5.90[a], 5.87[b]	65.5[d], 72[e]	4.59[c]	-	-	-
Other Theo. calculation		5.94[b], 5.95[c]	68[b],71[f], 60[g]	4.9[b], 4.41[g], 4.67[h]	5.71[b], 5.24[b]	-	-

[a]Ref[104], [b]Ref[105], [c]Ref[106], [d]Ref[107],[e]Ref[108], [f]Ref[109], [g]Ref[110], [h]Ref[111]

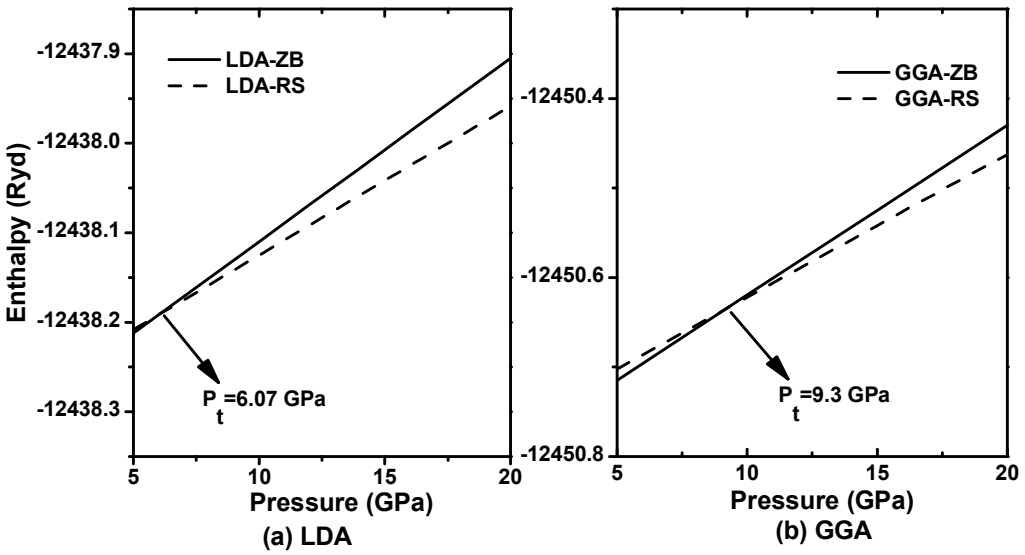

Figure. 4.8. Enthalpy as a function of pressure for ZB and RS phase of InP with (a) LDA method and (b) GGA method

Table 4.6. Phase transition pressure 'P_t(GPa)' and volume collapse of InP

	Present calculation	**Expt. results**	**Theoretical results**
Transition pressure (P_t)(GPa)	6.07 (LDA) 9 .3 (GGA)	9.5[a],10.3±0.2[b], 9.8[c]	7.3[d], 7.5[e], 8.5[f],11.0[g]
Volume collapse (%)	16.45	14.9[b]	18[f], 15[g],17[h]

[a]Ref[27], [b]Ref[28], [c]Ref[105], [d]Ref[25], [e]Ref[112], [f]Ref[93], [g]Ref[94], [h]Ref[113]

The enthalpy curve in figure 4.8 indicates the structural transition pressure of InP in ZB to RS structure at 6.07 GPa pressure with LDA method and at 9.3GPa pressure with GGA method. The volume collapse of InP (within GGA) is shown in figure 4.9 with a volume decrease of 16.45% indicating that the ZB phase is more compressible than the RS phase. A comparison of results is shown in table 4.6.

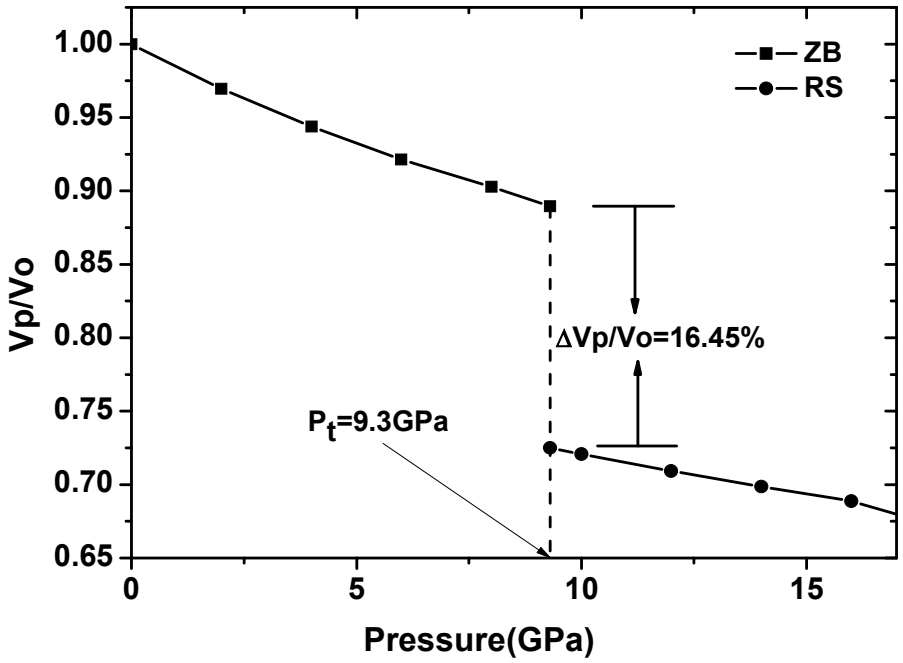

Figure 4.9. Normalized volume as a function of pressure for InP-ZB and InP-RS

(d) Indium Arsenide (InAs)

The structural stability and phase transition of InAs are studied in this subsection. The structural optimization curve of InAs is shown in figure 4.10 and shows more stability in ZB structure as compared to RS structure. The structural parameters for the present study and available experimental results are given in table 4.7. The transformation of ZB structure to RS structure of InAs under induced pressure takes place at 3.9GPa pressure and at 4.7GPa pressure with LDA, GGA method respectively as shown in the Enthalpy curve in figure 4.11. The volume collapse (in figure 4.12) in the phase transformation is found to have a volume decrease of 17.2% and implies that ZB phase is more compressible than the RS phase. Our calculated results of phase transition and volume collapse are compared with other experimental and theoretical results as shown in table 4.8.

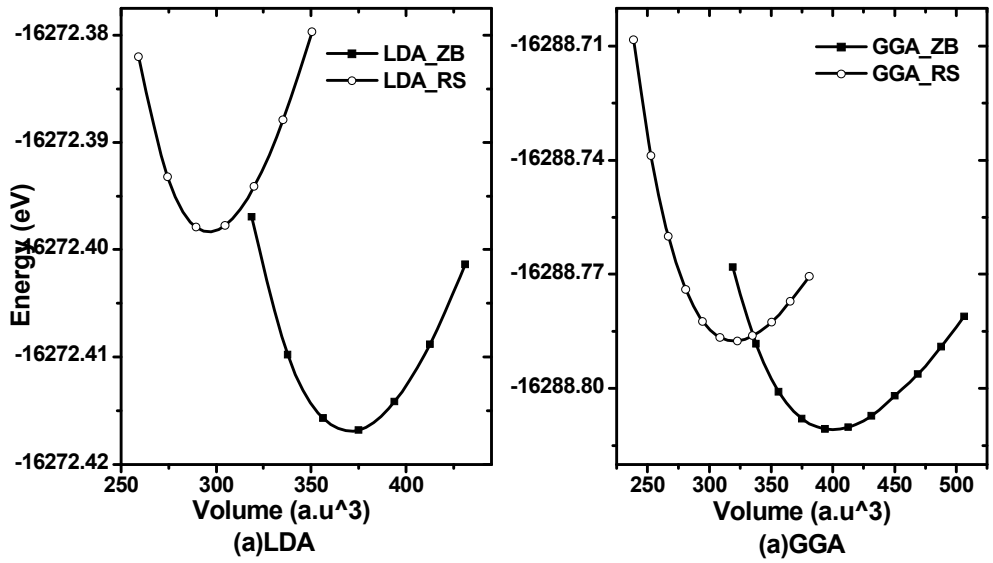

Figure 4.10. Total energy as a function of primitive cell volume for InAs-ZB and InAs-RS with (a) LDA method and (b) GGA method

Table 4.7. Experimental and calculated ground state structural parameters of InAS in ZB and RS structure

		Zinc Blende (ZB) Structure			**Rock Salt (RS) Structure**		
		a_0 (A^0)	B_0 (GPa)	$B^/$	a_0 (A^0)	B_0 (GPa)	$B^/$
Present work	LDA	6.03	61.3	4.86	5.60	77.604	4.96
	GGA	6.18	49.48	4.78	5.74	62.98,	4.84
Expt. work		6.10[a]	59.2±5[e]	6.8±2[e]	5.5005[e], 5.514[f]	40.6±14[e]	7.3±1[e]
Other Theo. calculation		6.10[b], 6.08[c]	55.51[c], 50.4[d]	-	5.65[c]	-	-

[a]Ref[81],[b]Ref[114],[c]Ref[115],[d]Ref[116],[e]Ref[117],[f]Ref[118].

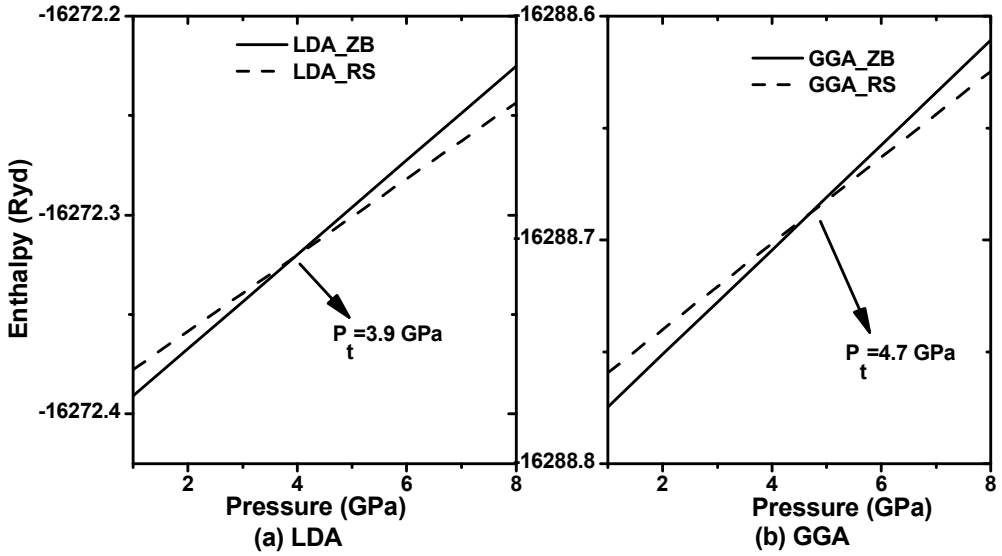

Figure. 4.11. Enthalpy as a function of pressure for ZB and RS phase of InAs with (a) LDA method and (b) GGA method

Table 4.8. Phase transition pressure 'P_t(GPa)' and volume collapse of InAs

	Present calculation	**Expt. results**	**Theo. results**
Transition pressure (P_t) (GPa)	3.9 (LDA) 4.7 (GGA)	7[a] , 6.9±0.2[b]	3.9[c], 4.0[d]
Volume collapse (%)	17.2	17.0±0.2[a], 18.8[b]	17.0[d]

[a]Ref[4], [b]Ref[117],[c]Ref[119],[d]Ref[120]

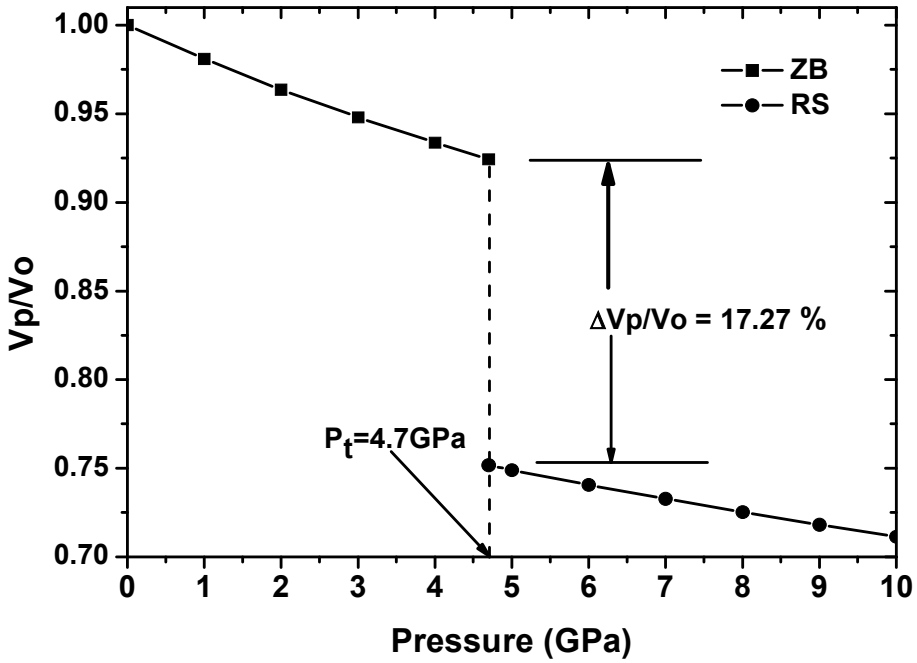

Figure 4.12. Normalized volume as a function of pressure for InAs-ZB and InAs-RS

4.3. ELASTIC PROPERTIES

The elastic constants play an important role in the study of relationship between crystal structures and bonding of a material. They give us important information about the nature of force operating in the solids and are basic parameters that are used for studying the elastic properties of a material. The mechanical stability condition of a crystal at high pressure can be understood from the pressure

dependence of the elastic constant. For a cubic crystal, the Born mechanical stability conditions are as follows: $(C_{11}+2C_{12}) > 0$; $C_{11}-C_{12} > 0$; $C_{11} > 0$; $C_{12} > 0$.

The Zener anisotropy factor (A), Poisson's ratio (υ), Kleinmann parameter (ξ), B/G ratio, Young's modulus (Y) and Debye's temperature (θ_D) are important parameters which determine the mechanical and thermal properties of a material. The elastic isotropy of a material is determined by the Zener Anisotropy factor (A). For A = 1, the material is elastically isotropic and deform uniformly along all directions of the body. If A > 1, it is stiffest along <111> plane body diagonals and when A < 1, it is stiffest along <100> cube axes. It is expressed as:

$$A = \frac{2C_{44}}{C_{11} - C_{12}} \tag{4.1}$$

The Poisson's ratio (υ), provides a sharp criterion for differentiating the brittleness and ductility in solids and give us information about the characteristics of bonding forces. For covalent materials υ=0.1 whereas for ionic materials, υ= 0.25 [121]. The upper and the lower limits of υ in central force solids have been reported to be 0.25 and 0.5 respectively [122]. It is calculated using the relation,

$$\upsilon = \frac{1}{2}\left(\frac{B - (2/3)G}{B + (1/3)G}\right) \tag{4.2}$$

where B is the Bulk modulus and G is the isotropic shear modulus as given by

$$G = \frac{G_V + G_R}{2} \tag{4.3}$$

G_v is the Voigt's shear modulus corresponding to the upper bound of G values, and G_R is the Reuss's shear modulus corresponding to the lower bound of G values. G_v and G_R can be expressed as:

$$G_V = \frac{C_{11} - C_{12} + 3C_{44}}{5} \tag{4.4}$$

$$G_R = \frac{5(C_{11} - C_{12})C_{44}}{4C_{44} + 3(C_{11} - C_{12})} \tag{4.5}$$

Kleinmann parameter (ζ) describes the relative position of the cation and anion sub-lattices and is given by the relation

$$\zeta = \frac{C_{11} + 8C_{12}}{7C_{11} + 2C_{12}} \tag{4.6}$$

It also implies resistance against bond bending or bond angle distortion. In a system, minimising bond bending leads to ζ=0 and minimising bond stretching leads to ζ=1.

The ductile and brittle behaviour of a material can be understood from the ratio of the bulk and shear modulus (B/G) [123]. If the shear modulus (G) is low we know that it has a low resistance to shear and hence is ductile while if a material has low bulk modulus, it means the resistance fracture is low and hence brittle. We know that the critical value which separates the ductility and brittleness of a material is 1.75. A material is said to be ductile if B/G > 1.75 and brittle if B/G < 1.75.

The Young's modulus is determined to measure the stiffness of the solid and is given by:

$$Y = \frac{9GB}{G + 3B} \tag{4.7}$$

Debye's temperature gives us explicit information about lattice vibrations and is also an important parameter determining the thermal characteristics of a material. It is calculated using the average sound velocity (υ_m) given by the relation [124]:

$$\theta_D = \frac{h}{k}\left[\frac{3n}{4\pi}\left(\frac{N_A\rho}{M}\right)\right]^{1/3}\upsilon_m \tag{4.8}$$

where h is the Plank's constant, k is the Boltzmann constant, N_A is the Avogadro's number, n is the number of atoms per formula unit, M is the molecular mass per formula unit, ρ is the density and υ_m is given by [125]:

$$\upsilon_m = \left[\frac{1}{3}\left(\frac{2}{\upsilon_t^3}+\frac{1}{\upsilon_l^3}\right)\right]^{-(1/3)} \tag{4.9}$$

where υ_t and υ_l are the transverse and longitudinal velocities respectively, which are obtained from Navier's equation as [126]:

$$\upsilon_l = \sqrt{\frac{3B+4G}{3\rho}} \tag{4.10}$$

$$\upsilon_t = \sqrt{\frac{G}{\rho}} \tag{4.11}$$

In the present study, the elastic constants, C_{11}, C_{12} and C_{44} at different pressures are calculated within the GGA only.

(a) Gallium Phosphide (GaP)

In the previous subsection, we have observed a phase transformation from zincblende (ZB) to rocksalt (RS) phase of GaP under induced pressure at 21.9 GPa pressure. Thus the elastic constants of GaP are calculated for the lattice corresponding to pressure ranging from 0 GPa to 20 GPa pressure for ZB structure and from 23 GPa to 37 GPa pressure for RS structure. We find that the present calculated results as shown in figure 4.13 satisfy the mechanical stability conditions: $(C_{11}+2C_{12}) > 0$; $C_{11}C_{12} > 0$; $C_{44} > 0$; $C_{11} > 0$ for the ZB and RS phases.

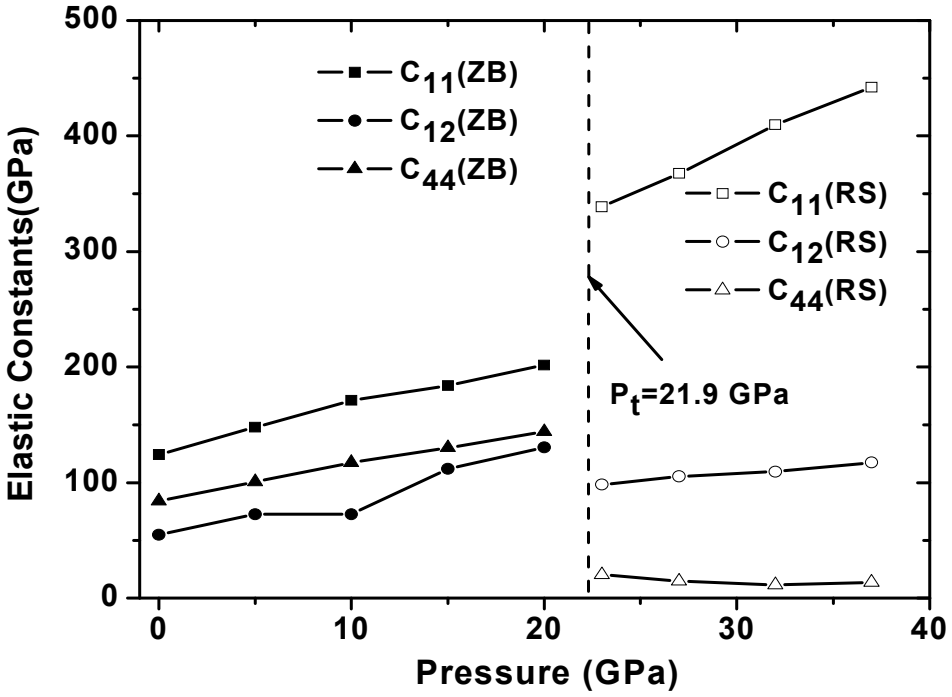

Figure 4.13. Elastic constants (C_{11}, C_{12}, C_{44}) as a function of pressure of GaP-ZB and GaP-RS phase

The elastic parameters such as Zener Anisotropy factor (A), Poisson's ratio (υ), kleinmann's parameter (ζ), B/G ratio, Young's modulus (Y) and Deby's temperature (θ_D) are calculated for both GaP-ZB and GaP-RS phases at different pressures to study mechanical and thermal behavior of GaP at high pressures.

In figure 4.14 the elastic parameters (Zener Anisotropy factor (A), Poisson's ratio (υ), kleinmann's parameter (ζ) and B/G ratio) as a function of pressure are given.

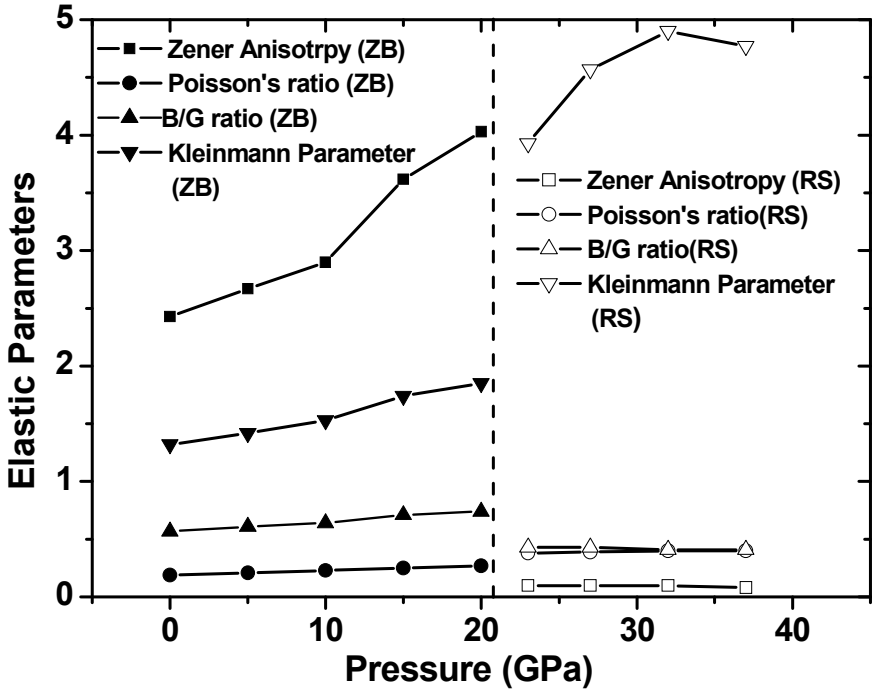

Figure 4.14. Elastic parameters (Zener Anisotropy factor, Poisson's ratio, Kleinmann parameter and B/G ratio) as a function of pressure for ZB and RS phases of GaP

Our calculation of the Zener Anisotropy factor (A) shows a variation from 2.43 to 4.03 in the ZB phase while in the RS phase it decreases from 0.16 to 0.08 with pressure. Thus we find that A is stiffest along <111> body diagonal in ZB phase and after transition to RS phase it becomes stiffest along <100> cube axes. Our results of Poisson's ratio (υ) shows that as pressure increases, the value of υ increases from 0.19 to 0.27 in ZB phase while it increases from 0.38 to 0.40 in RS phase indicating higher ionic contribution in the inter atomic bonding with increasing pressure. It also indicates with increasing pressure inter atomic forces tend to be more central. In the present study, the Kleinmann parameter (ζ) of the ZB phase is found to vary from 0.57 to 0.74 with pressure while in RS phase it is found to decrease from 0.43 to 0.41 showing shrinkage in bond stretching in the ZB phase and shrinkage in bond bending in the RS phase. We also find that with

increase in pressure the B/G ratio of GaP-ZB phase increases from 1.32 to 1.86 while the GaP-RS phase shows an increase from 3.93 to 4.77. Hence we conclude that the brittle nature of ZB phase of InAs becomes ductile as pressure increases and retains its ductility even after it undergoes a structural phase transition to RS phase.

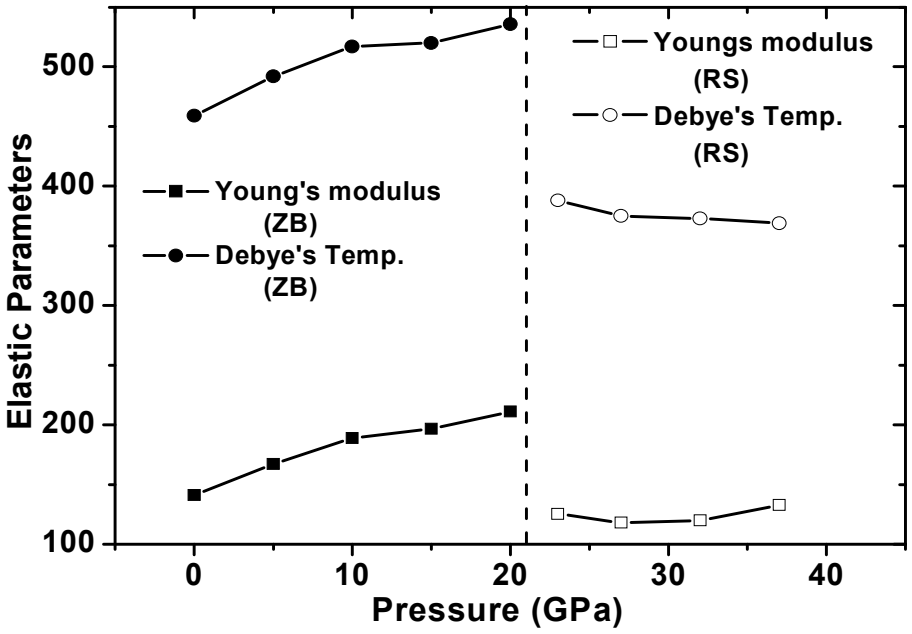

Figure 4.15. Elastic parameters (Young's modulus and Debye's temperature) as a function of pressure of GaP in ZB phase and RS phase

The elastic parameters (Young's modulus and Debye's temperature) as a function of pressure of both GaP-ZB and GaP-RS phases are shown in figure 4.15. From the figure it is observed that with increase in pressure the value of Y increases from 141.06 GPa to 210 GPa in ZB phase while in RS phase the value of Y at first decreases from 125.29 GPa to 117. 86 GPa and then increases to 132.61 GPa. Thus GaP becomes more rigid with increase in pressure in ZB phase but after it undergoes a structural transformation to RS phase, the rigidity of GaP slightly decreases at certain pressure but soon attains its rigidity again as pressure goes on increasing. As the pressure increases, the value of Debye's temperature also

increases from 459 K to 536 K for ZB phase indicating stiffer lattice and better thermal conductivity but after undergoing structural transformation to RS phase the temperature decreases from 388 K to 369 K indicating weaker lattice and decrease in thermal conductivity.

(b) Gallium Arsenide (GaAs)

The transition pressure of GaAs for ZB to RS phase is found as 10.7 GPa pressure as shown in the previous subsection. Figure 4.16 shows the elastic constants (C_{11}, C_{12}, C_{44}) of Gallium Arsenide (GaAs) under pressure 0 GPa to 10 GPa pressure for ZB structure and 12 GPa to 20 GPa pressure for RS structure. It is noted that the mechanical stability conditions are found to satisfy for the ZB phase only and not for the RS phase. In the figure 4.16, there is a linear variation of elastic constants with pressure up to 10 GPa pressure in ZB phase while in the RS phase the value of C_{44} are found less than 0 GPa which indicates the instability of the RS phase at higher pressures. Therefore the elastic parameters at higher pressures are studied only for the ZB phase.

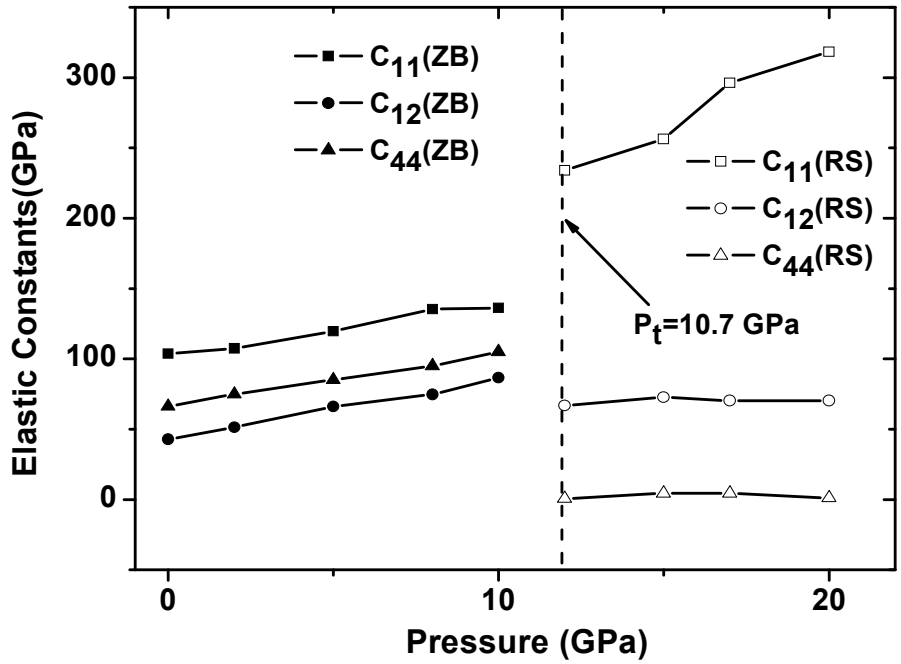

Figure 4.16. Elastic constants (C_{11}, C_{12}, C_{44}) as a function of pressure of GaAs-ZB and GaAs-RS phase

Figure 4.17 shows the elastic parameters (Zener Anisotropy factor, Poisson's ratio, Kleinmann parameter and B/G ratio) as a function of pressure of GaAs in ZB phase. The Zener Anisotropy factor (A) shows a variation from 2.17 to 4.22 in the ZB phase thus A is stiffest along <111> body diagonal in the ZB structure. The Poisson's ratio (υ) shows that the value of υ increases from 0.18 to 0.25 indicating higher ionic contribution in inter atomic bonding with increasing pressure. It also indicates that with increasing pressure inter atomic forces tend to be more central. The Kleinmann parameter (ζ) of the ZB phase is found to vary from 0.55 to 0.73 with pressure showing bond stretching in the ZB phase. The B/G ratio of ZnS-ZB phase increases from 1.26 to 1.73. Hence we conclude that the brittle nature of GaAs in ZB structure becomes ductile as the pressure increases.

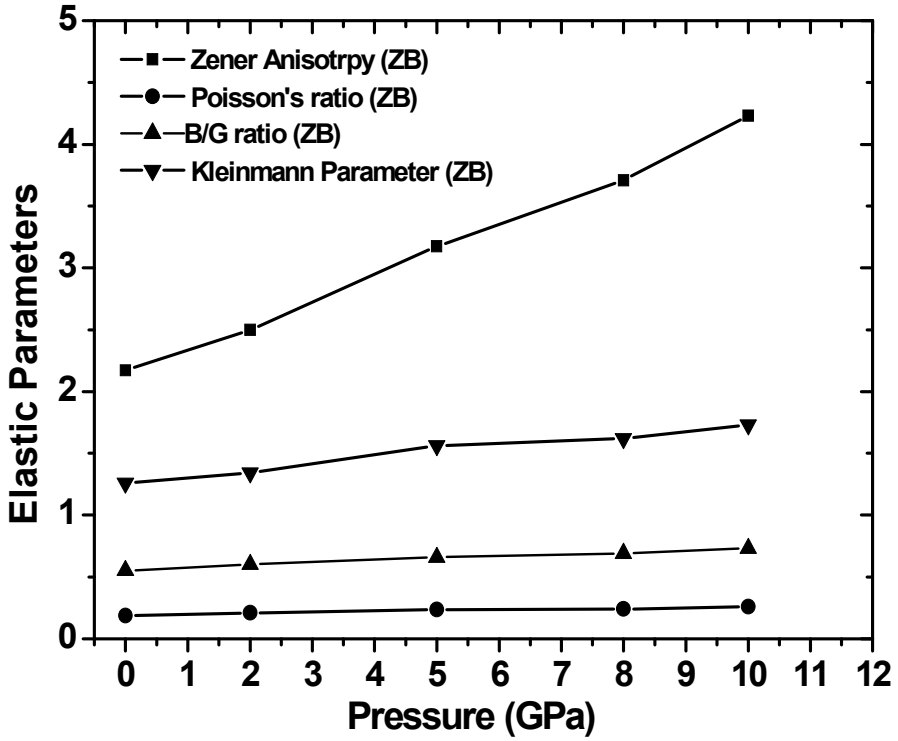

Figure 4.17. Elastic parameters (Zener Anisotropy factor, Poisson's ratio, Kleinmann parameter and B/G ratio) as a function of pressure of GaAs in ZB phase

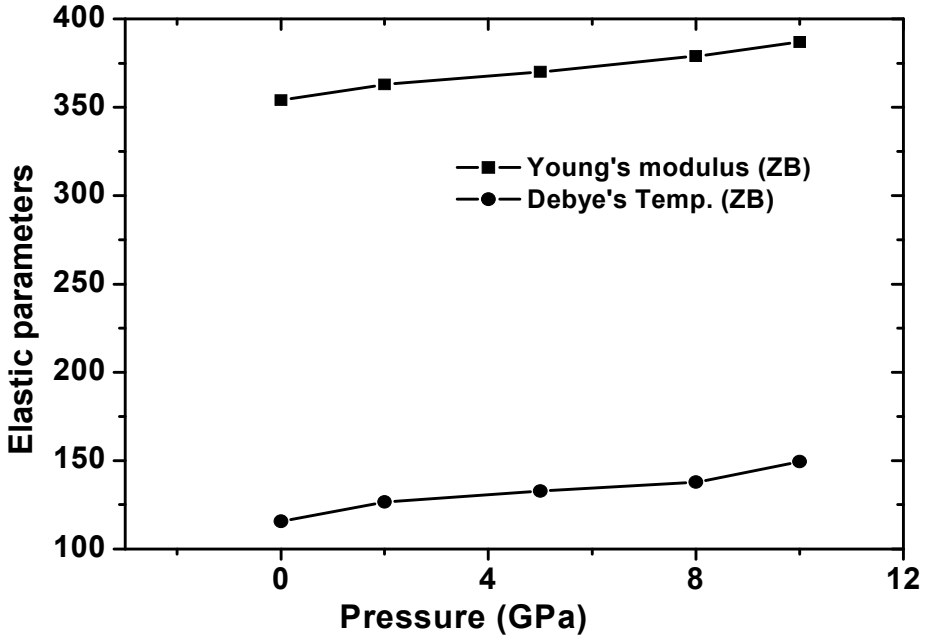

Figure 4.18. Elastic parameters (Young's modulus and Debye's temperature) as a function of pressure of GaAs in ZB phase

The elastic parameters (Young's modulus and Debye's temperature) as a function of pressure of ZnS-ZB are shown in figure 4.18. From the figure it is seen that with increase in pressure the value of Y increases from 115.73 GPa to 149.45 GPa in ZB phase. Thus in ZB phase, GaAs becomes more rigid with increase in pressure. As the pressure increases, the value of Debye's temperature also increases from 354 K to 387 K indicating stiffer lattice and better thermal conductivity of GaAs-ZB phase.

(c) Indium Phosphide (InP)

As calculated above the transition pressure of InP-ZB to InP-RS structure is 9.3 GPa, therefore the elastic constants are calculated for Indium phosphide (InP) ranging from 0 GPa to 8 GPa pressure for ZB and from 10 GPa to 16 GPa pressure for RS (figure 4.19). The obtained results are found to be satisfying the mechanical stability conditions for both the phases. Hence the elastic parameters of InP under

high pressure are calculated for both ZB and RS phases. The elastic parameters (Zener Anisotropy factor (A), Poisson's ratio (υ), kleinmann's parameter (ζ) and B/G ratio) are shown in figure 4.20.

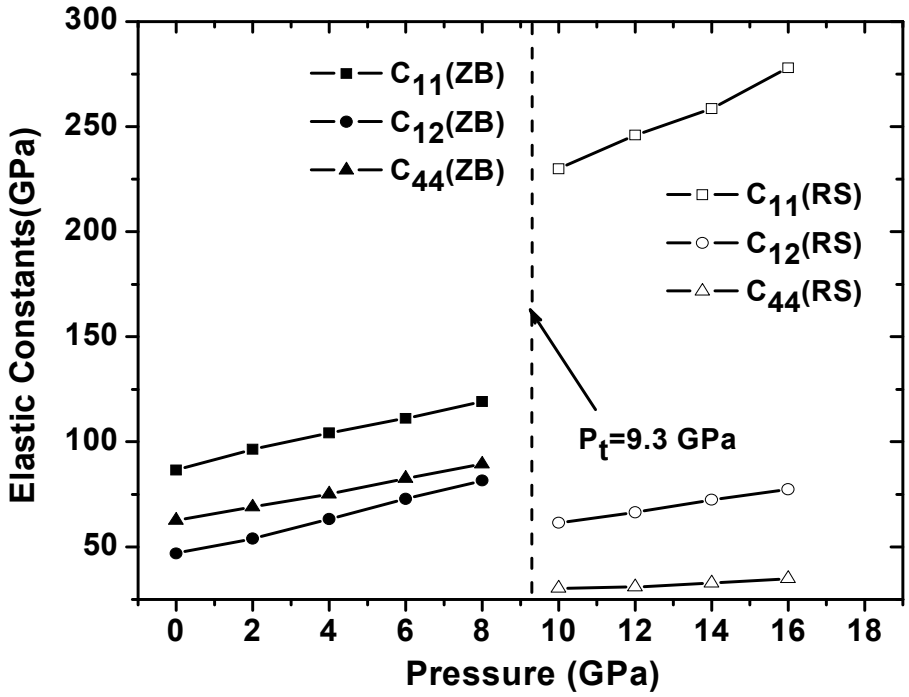

Figure 4.19. Elastic constants (C_{11}, C_{12}, C_{44}) as a function of pressure of InP-ZB and InP-RS phase

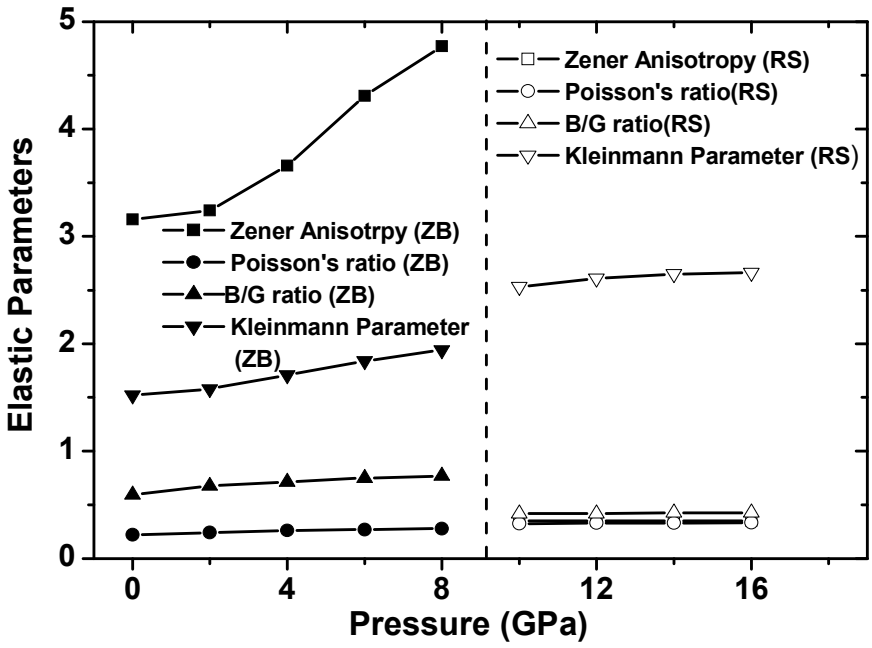

Figure 4.20. Elastic parameters (Zener Anisotropy factor, Poisson's ratio, Kleinmann parameter and B/G ratio) as a function of pressure of InP-ZB phase and InP-RS phase

Zener Anisotropy factor (A) shows a variation from 3.16 to 4.77 and 0.35 to 0.36 with increase in pressure of ZB and RS phase respectively and thus showing the degree of elastic anisotropy. Thus A is stiffest along <111> body diagonal in the ZB phase and after transition to RS phase it becomes stiffest along <100> cube axes. As pressure increases, the value of Poisson's ratio (υ) increases from 0.22 to 0.28 in ZB phase while it increases from 0.32 to 0.33 in RS phase indicating higher ionic contribution in the inter atomic bonding with increasing pressure and also indicates that with increasing pressure inter atomic forces tend to be more central. The Kleinmann parameter (ζ) of t ZB phase is found to increase from 0.59 to 0.77 with pressure while in RS phase it is found to increase from 0.41 to 0.42 showing shrinkage in bond stretching in both ZB and RS phases. As pressure increases the B/G ratio of InP-ZB phase increases from 1.52 to 1.94 while in InP-RS phase it increases from 2.5 to 2.6. Hence we conclude that the brittle nature of the ZB phase

of InP becomes ductile as the pressure increases and retains its ductility even after it undergoes a structural phase transition to RS phase.

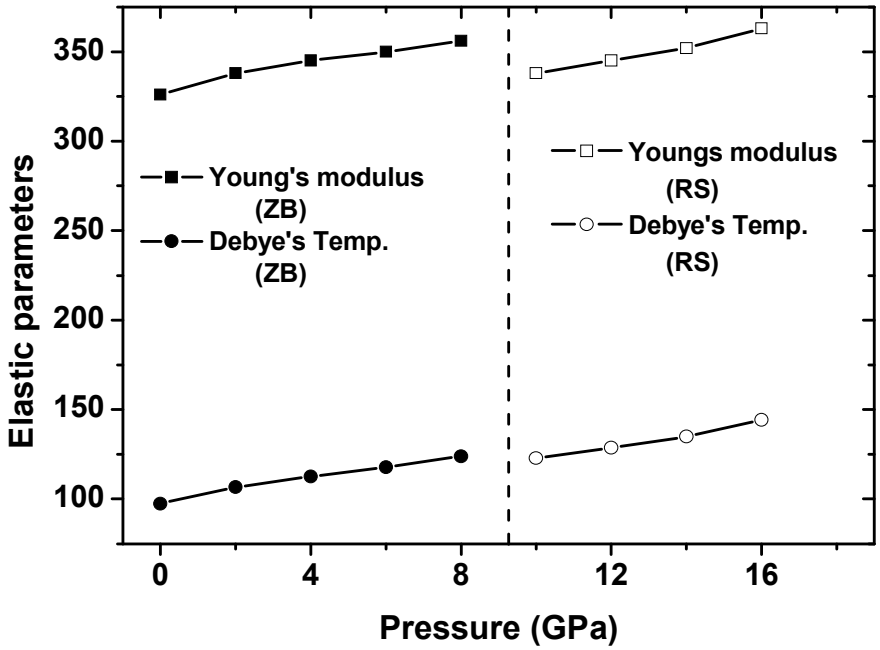

Figure 4.21. Elastic parameters (Young's modulus and Debye's temperature) as a function of pressure of InP in ZB phase and RS phase

It is seen in figure 4.21, with increase in pressure the value of Y increases from 97.48 GPa to 123 GPa in the ZB phase while in the RS phase the value of Y increases from 122.85 GPa to 144.36 GPa. Thus it is interesting to note that InP becomes more rigid with increase in pressure in ZB phase and even after it undergoes a structural transformation to RS phase the rigidity of InP is maintained. The increase in Debye's temperature with increasing pressure in figure 4.21, indicates stiffer lattice and better thermal conductivity under pressure in both the phases.

(d) Indium Arsenide (InAs)

Similarly as in above subsections, the elastic constants have been calculated for 0 GPa to 4 GPa pressure of InAs-ZB and from 5 GPa to 9 GPa pressure of InAs-RS as the structural phase transition of InAs from the zincblende to rocksalt occurs at 4.7 GPa pressure. The calculated elastic constants in figure 4.23 satisfy the mechanical stability conditions and are shown in figure 4.22. In figure 4.23, the elastic parameters (Zener Anisotropy factor (A), Poisson's ratio (υ), Kleinmann's parameter (ζ) and B/G ratio) are given.

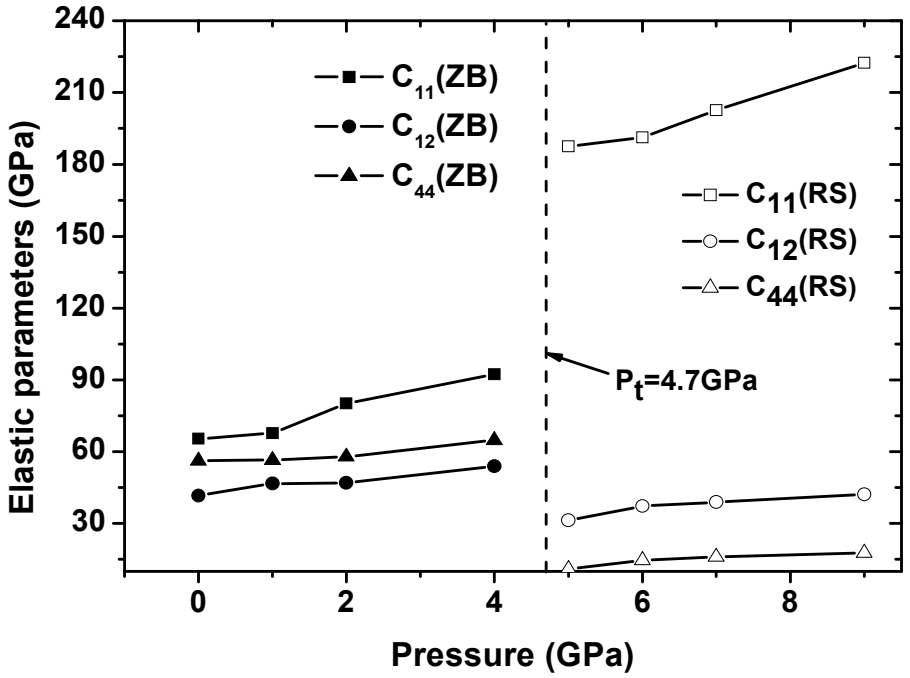

Figure 4.22. Elastic constants (C_{11}, C_{12}, C_{44}) as a function of pressure of InAs-ZB and InAs-RS phase

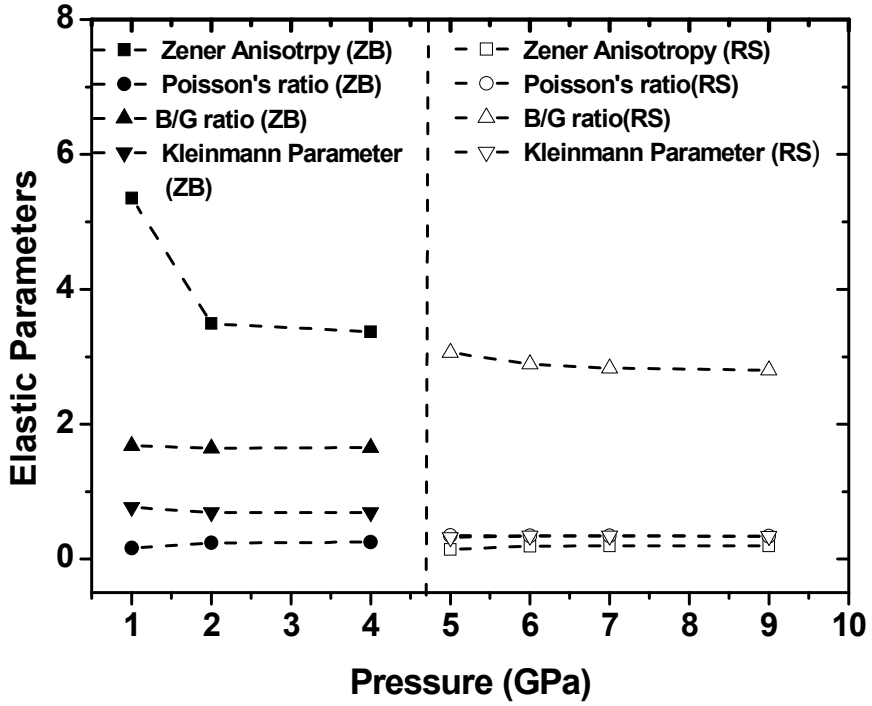

Figure 4.23. Elastic parameters (Zener Anisotropy factor, Poisson's ratio, Kleinmann parameter and B/G ratio) as a function of pressure of InAs in ZB phase and RS phase

It is seen that Zener Anisotropy factor (A) varies from 5.35 to 3.37 in the ZB phase while in the RS phase it is found to increase from 0.18 to 0.2. Thus A is stiffest along <111> body diagonal in the ZB phase and after transition to RS phase it becomes stiffest along <100> cube axes. There is an increase in the value of υ from 0.16 to 0.25 in ZB phase while it remains unchanged around 0.34 in the RS phase indicating dominant nature in the ionic contribution to the inter atomic bonding. The Kleinmann parameter (ζ) of ZB phase is found to vary from 0.77 to 0.69 with pressure while in RS phase it is found to increase from 0.31 to 0.34 showing shrinkage in bond stretching in the ZB phase and shrinkage in bond bending in the RS phase. With increase in pressure, the B/G ratio of InAs-ZB remains around 0.64 while in InAs-RS phase it is greater than 1.75 and then decreases.

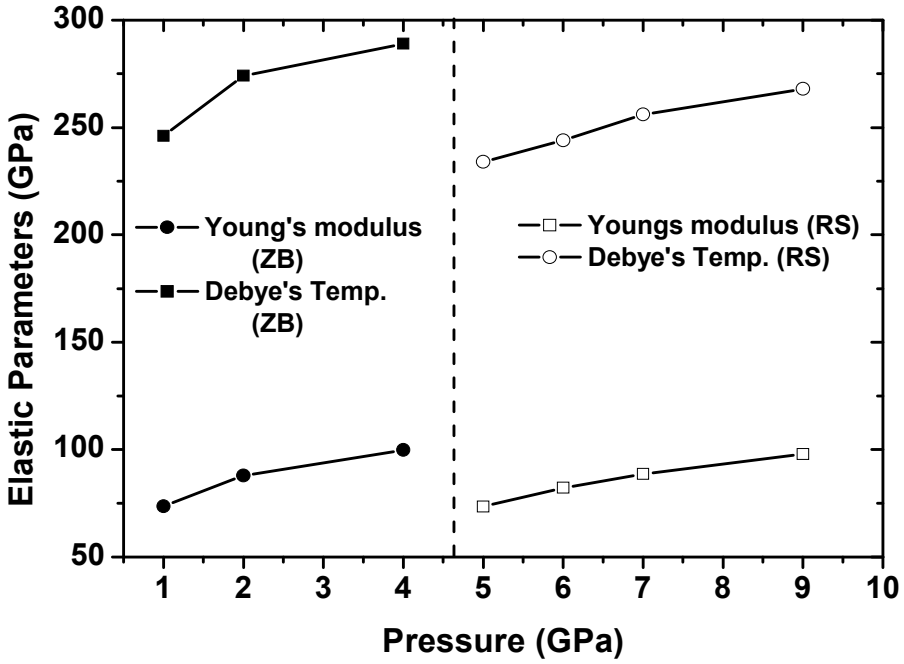

Figure 4.24. Elastic parameters (Young's modulus and Debye's temperature) as a function of pressure of InAs in ZB phase and RS phase

In figure 4.24, Young's modulus (Y) and Debye's temperature (θ_D) as a function of pressure are shown. As the pressure increases, the value of Y increases from 73.62 GPa to 99.72 GPa in the ZB phase while in the RS phase also the value of Y increases from 73.53 GPa to 97.84 GPa. Thus InAs becomes more rigid with increase in pressure in both the ZB and RS. As the pressure increases, the value of Debye's temperature also increases from 246 K to 290 K for the ZB phase and from 243K to 268 K in the RS phase indicating stiffer lattice and better thermal conductivity in both phases.

4.4. ELECTRONIC PROPERTIES

(a) Gallium Phosphide (GaP)

The electronic band structure calculation of GaP-ZB phase and GaP-RS phase at zero pressure (0 GPa) are performed with the methods (a) LDA, (b) GGA and (c)

mBJ-GGA and are shownin figure 4.25 and figure 4.26 respectively. In figure 4.25(a), (b) and (c) it is clearly seen that in all the three calculations within LDA, GGA and mBJ-GGA methods, the valence band maximum occurs at the Γ point while the minimum conduction band occurs at L point confirming an indirect band gap. One interesting point is the shifting of the conduction band towards higher energy and wide opening of the band gaps. The band gap calculated with LDA and GGA methods show a band gap of 1.46eV and 1.49eV respectively while calculation with mBJ-GGA method gives a band gap of 2.33eV which is very close to the experimental values of 2.32eV [101]. The order of the energy band gaps of GaP is LDA < GGA < mBJ-GGA. Thus the implementation of the mBJ-GGA potential resolves the underestimation of the band gaps and provides better results closer to the experimental value. Again in figure 24.6(a), (b) and (c), there is crossing over of the conduction band at the Fermi energy towards the valence band indicating metallic nature of GaP-RS phase. The metallic nature of GaP-RS structure is due to broadening of the band with increase in pressure and overlapping of the filled valence band and conduction band.

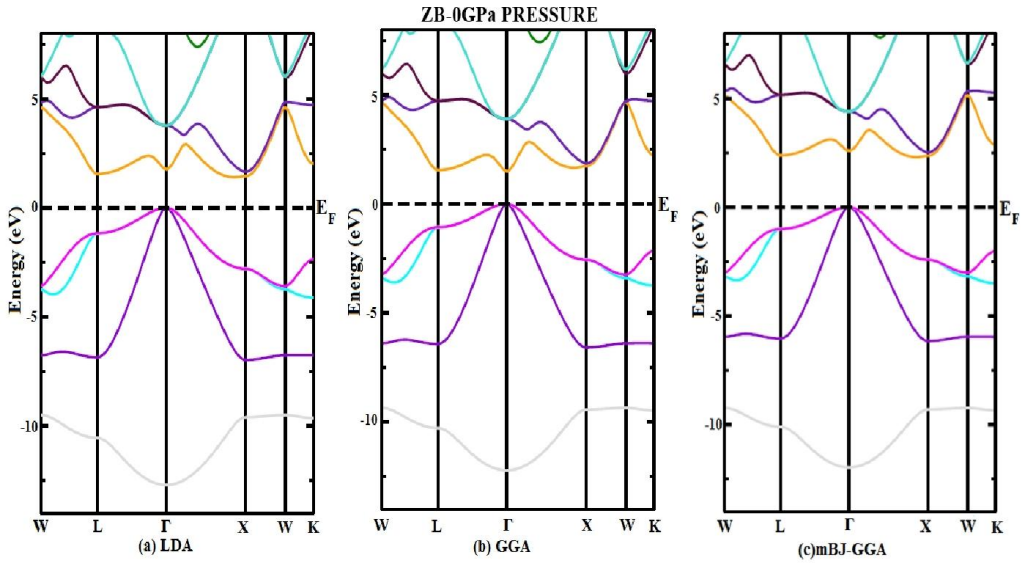

Figure 4.25. Energy band diagram of GaP-ZB phase at 0 GPa pressure within (a) LDA, (b) GGA and (c) mBJ-GGA

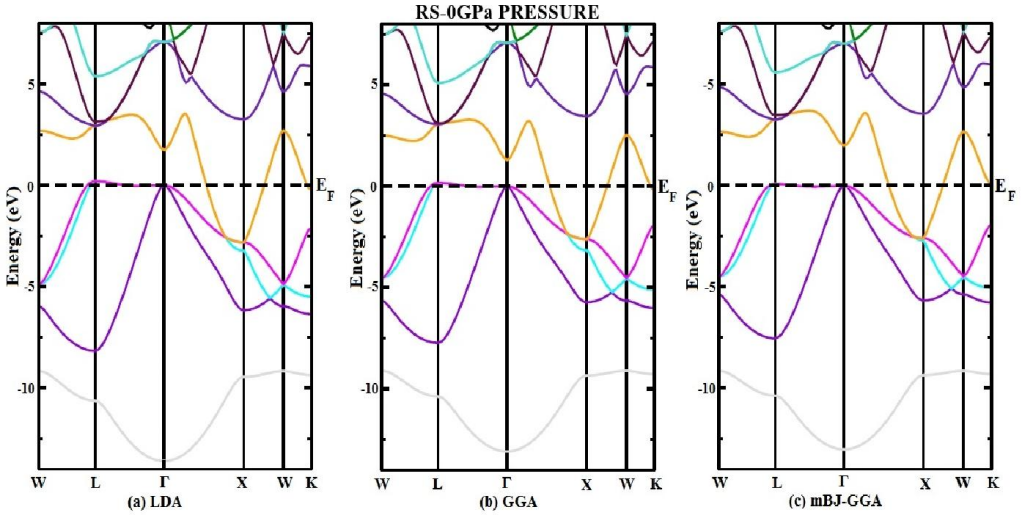

Figure 4.26. Energy band diagram of GaP-RS phase at 0 GPa pressure within (a) LDA, (b) GGA and (c) mBJ-GGA

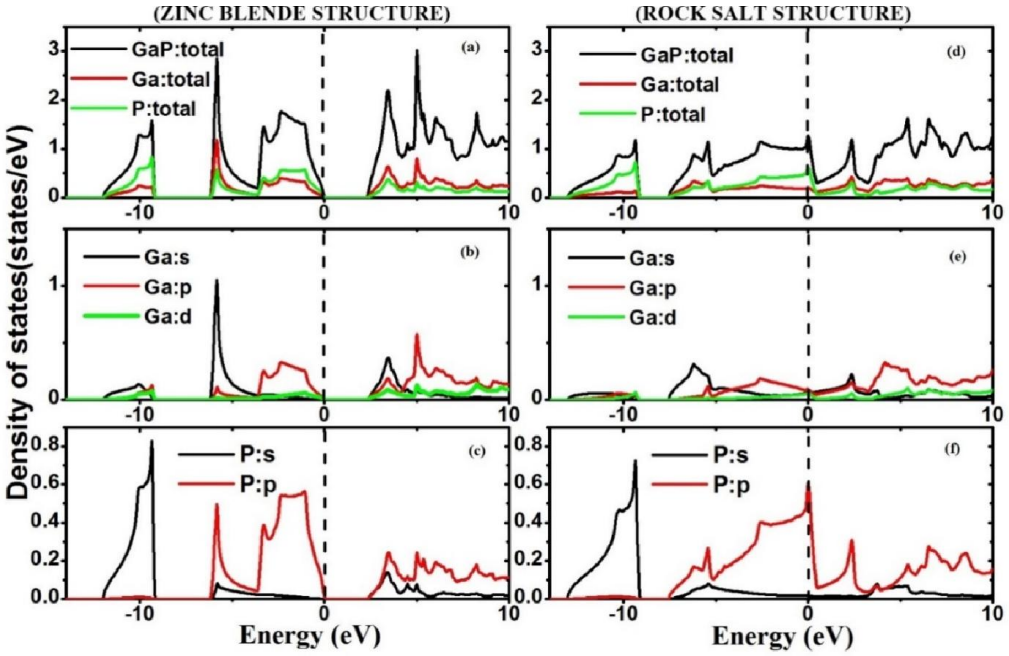

Figure 4.27. Total and Partial DOS of GaAS-ZB and GaAs-RS phase within mBJ-GGA

The nature of the energy band structure of a compound is related to the corresponding density of states. Therefore for better understanding of band gaps the total and partial density of states (DOS) are studied. But as we observed, the

calculations within the mBJ-GGA (as compare to LDA, GGA methods) gives us better results close to experimental value, we have calculated the total DOS and partial DOS with mBJ-GGA only. In figure 4.27, the total and partial DOS of GaP-ZB and GaP-RS are shown. Figure 4.27(a), (b) and (c) clearly show that the lowest band appears in energy band diagram (figure 4.26) is mainly contributed from s-non metal (P atom) orbital with little contribution from the p-metal (Ga atom) orbital and d-metal of (Ga atom) orbital while the valance band is mainly contributed by the s-metal (Ga-atom) orbital along with p-metal (Ga-atom) orbital and s-non metal (P atom) orbital with little contribution from the s-non metal (P-atom) orbital. Further the lowest band is mainly contributed by the s-non metal (P atom) orbital with little contribution from the p-metal (Ga-atom) orbital and d-metal (Ga-atom) orbital while the valance band is mainly contributed by the p-non metal (P-atom) orbital along with s-metal (Ga-atom) orbital and p-metal (Ga-atom) orbital. Other than the band structure at zero pressure, it is interesting to study how the band diagram changes under variation of pressures. In the following, we study the variation of band diagram under induce pressure of GaP-ZB phase and GaP-RS phase separately.

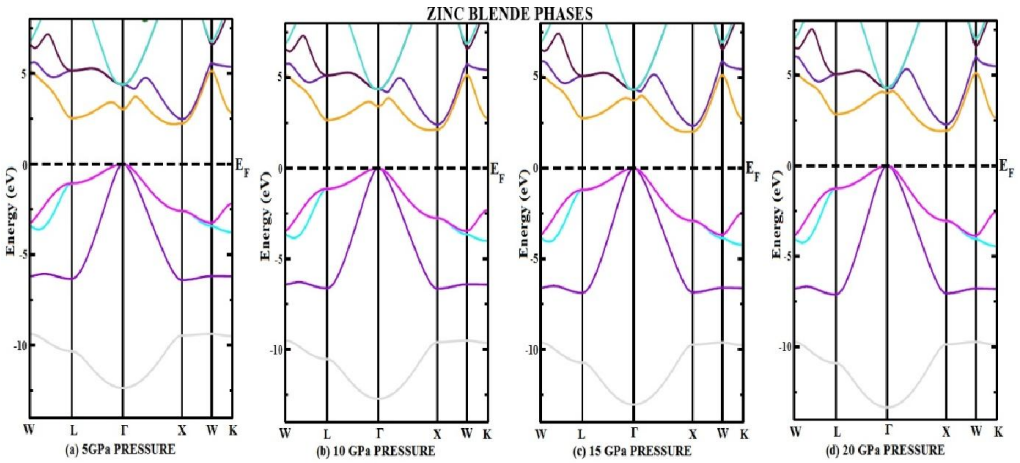

Figure 4.28. Energy band diagram of GaP-ZB phase at (a) 5 GPa pressure (b) 10 GPa pressure (c) 15 GPa pressure and (d) 20 GPa pressure

Figure 4.28 (a),(b),(c) and (d) show the energy band diagram of GaP-ZB at different pressures 5 GPa, 10 GPa, 15 GPa and 20 GPa. In figure 4.28 (a-d), it is observed that as the pressure increases to 5 GPa, 10 GPa 15 GPa and 20 GPa, the gap between the Γ-L increases but if we closely study the energy band diagram we find that the gap between Γ-X decreases towards the Fermi level indicating possibilities of crossing over of the conduction band towards the valance band at higher pressure confirming the metallic nature at higher pressure. The variation in the energy band gap with pressure is also shown in figure 4.29 for clear analysis of changes between Γ-X and Γ-L with pressure.

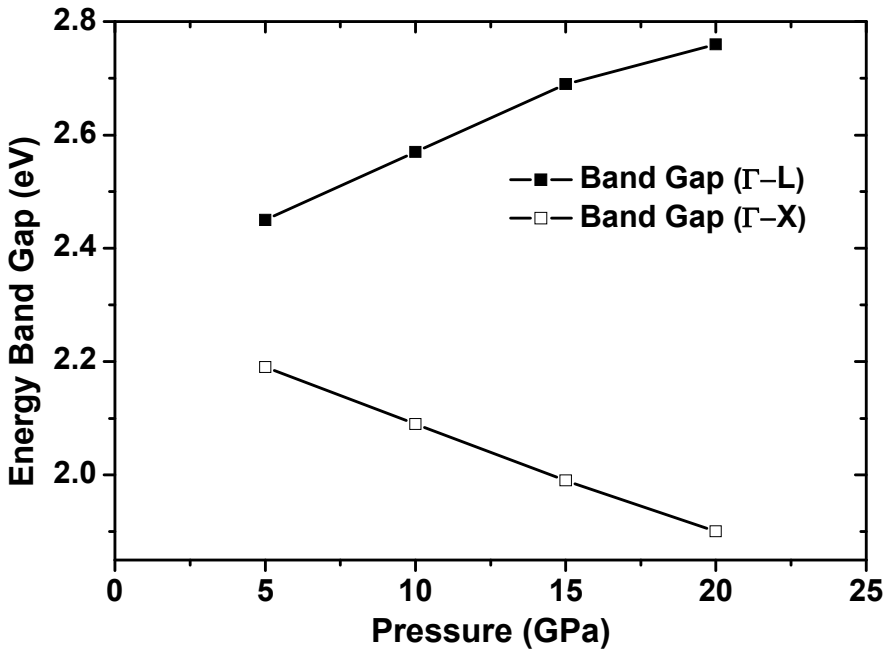

Figure 4.29. Variation of Energy band gaps of GaP-ZB phase with pressure

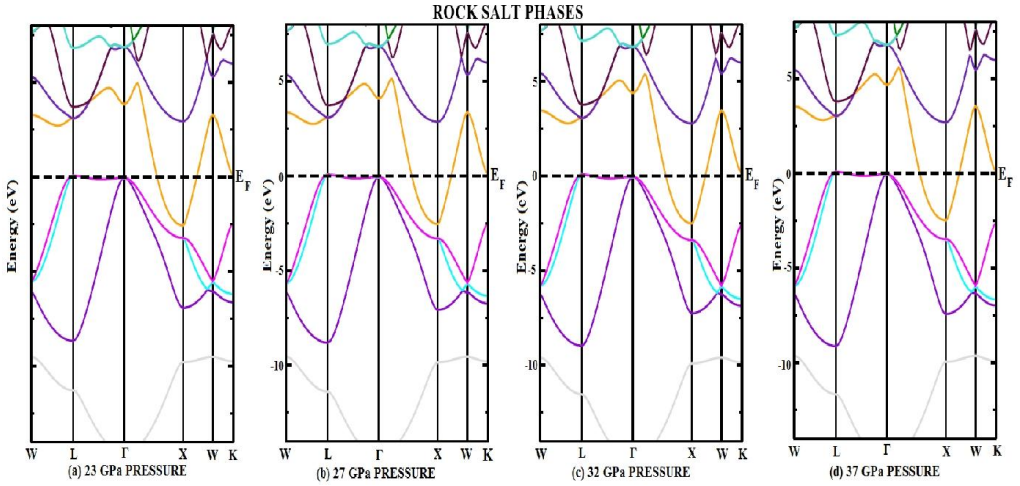

Figure 4.30. Energy band diagram of GaP-RS phase at (a) 23 GPa pressure (b) 27 GPa pressure (c) 32 GPa pressure and (d) 37 GPa pressure

In the similar way, we study the variation of band structure with pressure of GaP-RS phase. Figure 4.30 (a), (b), (c) and (d) show the energy band diagram of GaP-RS phase at 23 GPa, 27 GPa, 32 GPa and 37 GPa pressure respectively. From the figures, it is clearly seen that the metallic nature is retained even at high pressure. Hence we conclude that the energy band gap of GaP-ZB phase is affected by pressure while the energy band gaps of GaP-RS phase is not much affected by pressure.

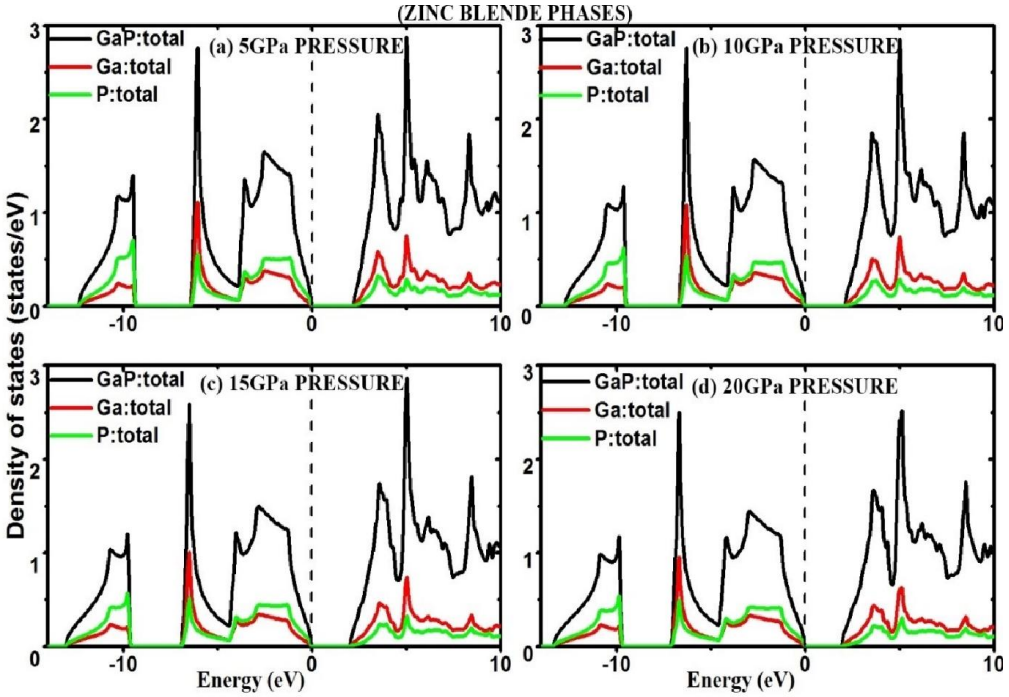

Figure 4.31. Total DOS of GaP-ZB at (a) 23 GPa pressure (b) 27 GPa pressure (c) 32 GPa pressure and (d) 37 GPa pressure

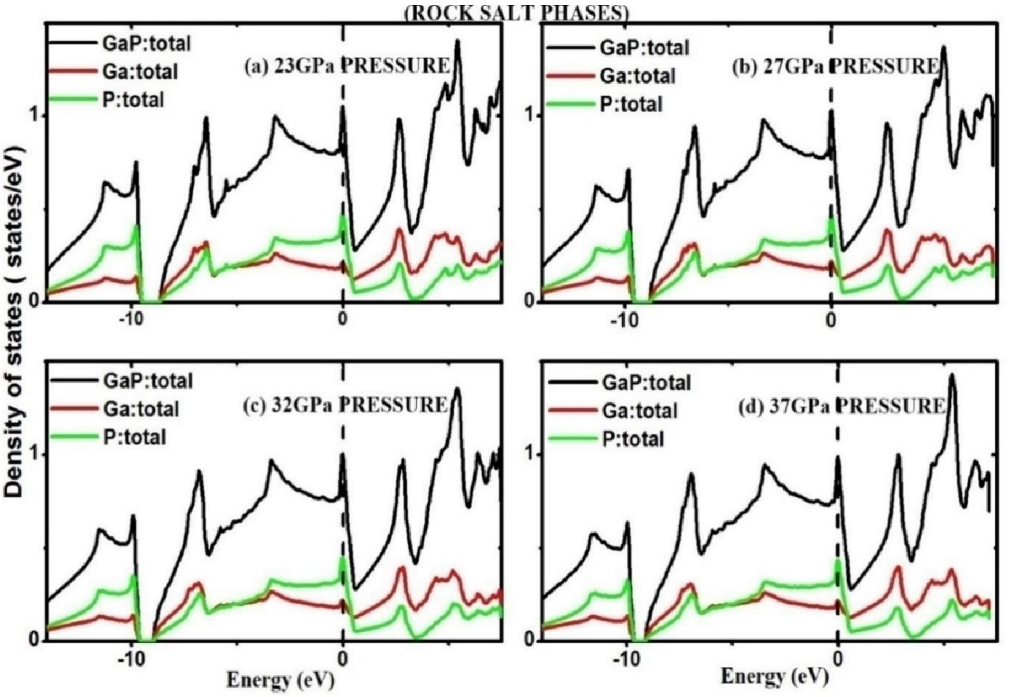

Figure 4.32. Total DOS of GaP-RS at (a) 23 GPa pressure (b) 27 GPa pressure (c) 32 GPa pressure and (d) 37 GPa pressure

To understand the effect of pressure in the band structures, we study the total DOS of GaP-ZB and GaP-RS at different pressure. Figure 4.31 shows the total DOS of GaP-ZB at (a) 5 GPa pressure (b) 10 GPa pressure (c) 15 GPa pressure and (d) 20 GPa pressure. From the DOS figures, we could clearly observe the gap (between Γ-X in band diagram figure 4.30) between the valence band and conduction band around the Fermi line (vertical dotted lines at 0 eV on the X-axis). Further it clearly also shows a slight increase of the wide of gap with increase in pressure.

In figure 4.32, the total DOS of GaP-RS at (a) 23 GPa pressure (b) 27 GPa pressure (c) 32 GPa pressure and (d) 37 GPa pressure are shown. The characteristic feature of metallic nature in the band diagram (figure 4.30), is clearly also reflected in DOS plot. Figure 4.32 shows orbital crossing the Fermi level and hence there is crossover of valence and conduction band. Thus GaP-RS phase retains its metallic nature under induced pressures.

4.4.2. Gallium Arsenide (GaAs)

Following the same methodology of band structure calculation as done for GaP in the previous subsection, Figure 4.33 show the electronic band structure of GaAs-ZB and GaAs-RS at 0 GPa pressure. In figure 4.33 of GaAs-ZB phase, calculations with the three methods: LDA, GGA and mBJ-GGA, show a direct band gap. The band gap calculated with LDA and GGA show a band gap of 0.17eV and 0.45 eV respectively while calculation within mBJ-GGA gives a band gap of 1.3eV which is very close to the experimental values of 1.5eV [101]. In figure 4.34 of GaAs-RS phase, the crossing over of the conduction band at the Fermi energy towards the valance band predicts the metallic nature of GaP-RS phase. The metallic nature of GaAs-RS is due to broadening of the band and overlapping of the filled valance band and conduction band.

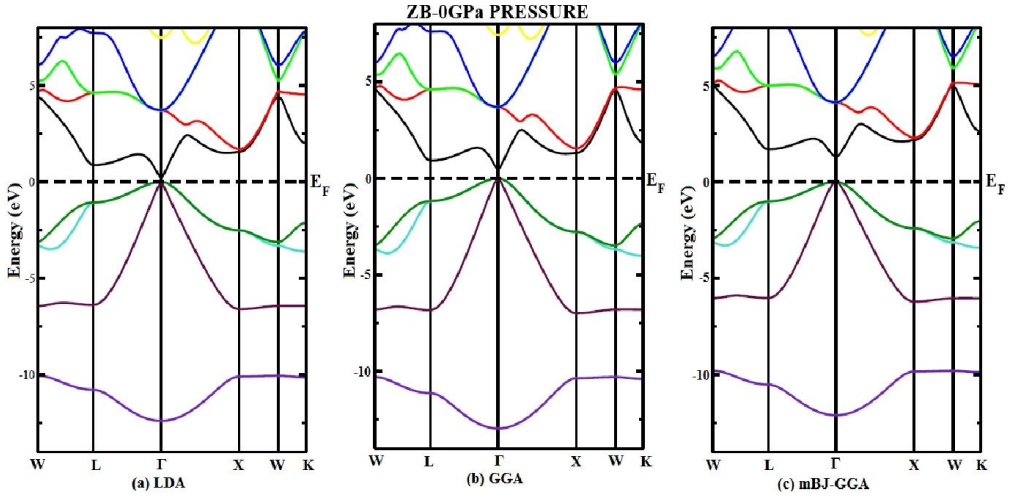

Figure 4.33.Band structure of GaAs-ZB at 0 GPa pressure within (a) LDA, (b) GGA and(c) mBJ-GGA

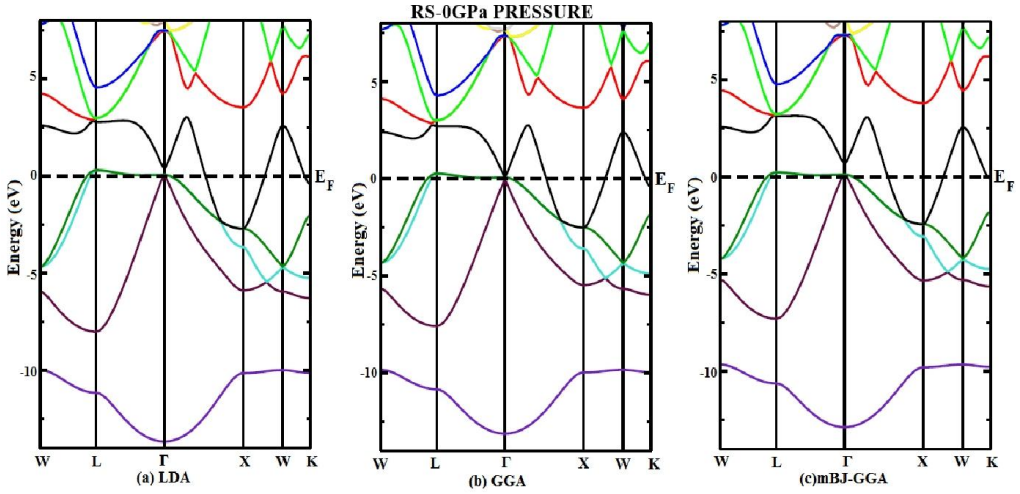

Figure 4.34. Band structure of GaAs-RS at 0 GPa pressure within (a) LDA, (b) GGA and (c) mBJ-GGA

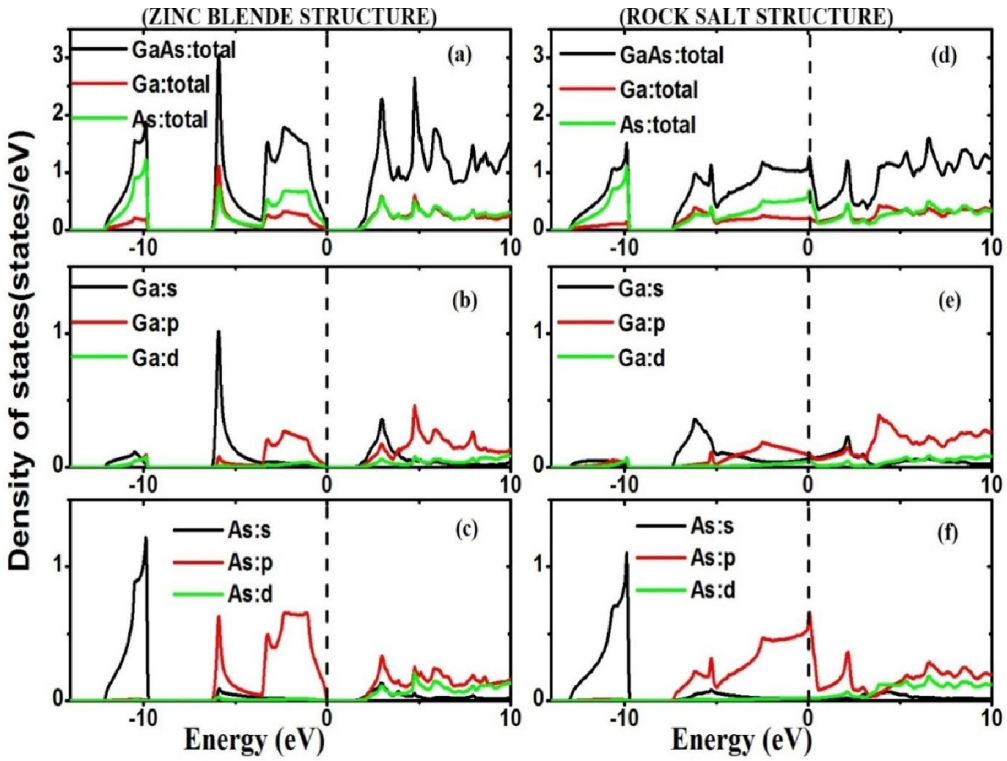

Figure.4.35. Total and Partial DOS of GaAS-ZB and GaAs-RS within mBJ-GGA

As mentioned above, the origin of the energy band structure of a compound is related to the corresponding density of states. In figure 4.35, the total and partial DOS of GaAs-ZB and GaAs-RS are shown. From figure 4.35(a), (b) and (c), for GaAs-ZB, we find that the lowest band is mainly contributed by the s-non metal (As atom) orbital while the valance band is mainly contributed by the s-metal (Ga atom) orbital with little contribution from the p-metal (Ga-atom) orbital. Again from figure 4.35(d),(e) and (f) for GaAs-RS we find that the lowest band is mainly contributed by the s-non metal (As atom) orbital with little contribution from the p-metal (Ga-atom) orbital and d-metal (Ga-atom) orbital while the valance band is mainly contributed by the p-non metal (As-atom) orbital and s-metal (Ga-atom) orbital with little contribution from the p-metal (Ga-atom) and d-metal (Ga-atom) orbital.

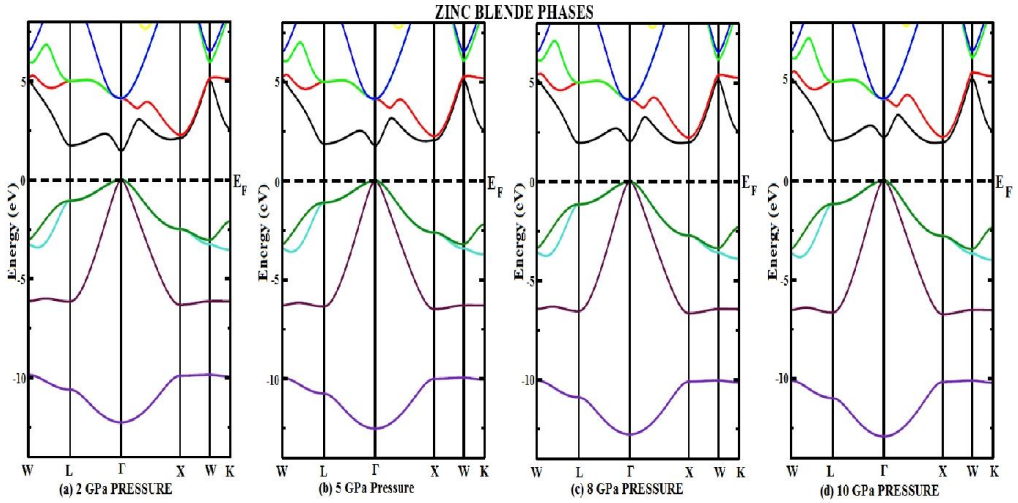

Figure 4.36. Energy band diagram of ZB phase of GaAs at (a) 2 GPa pressure (b) 5 GPa pressure (c) 8 GPa pressure and (d) 10 GPa pressure

Variation of band diagrams at various pressures of GaP-ZB structure are shown in figure 4.36(a),(b),(c) and (d). As the pressure increases to 2GPa, 5GPa, 8GPa and 10 GPa, the gap between the Γ- Γ point increases but if we closely study the energy band diagram we find that there is an increases in the gap between Γ-L point while the gap between Γ-X decreases. It predicts the possibility of crossing over Fermi level at higher pressure and phase transformation may take place to RS structure. The variation in the energy band gap with pressure for GaAs-ZB is also shown in figure 4.37 for clear analysis of the changes in the gap between Γ- Γ point, Γ-X point and Γ-L point.

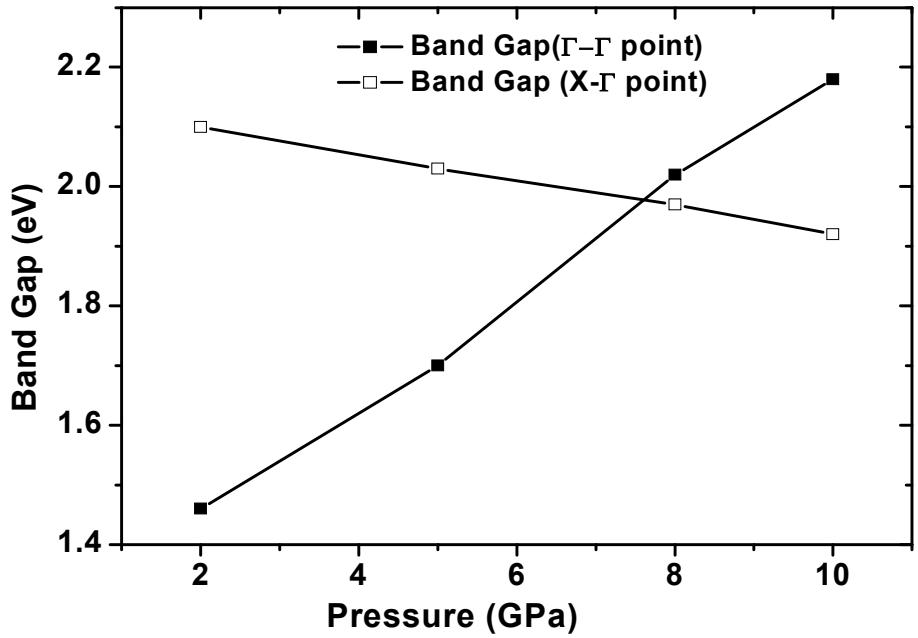

Figure 4.37. Variation of Energy band gaps of GaAs-ZB phase with pressure

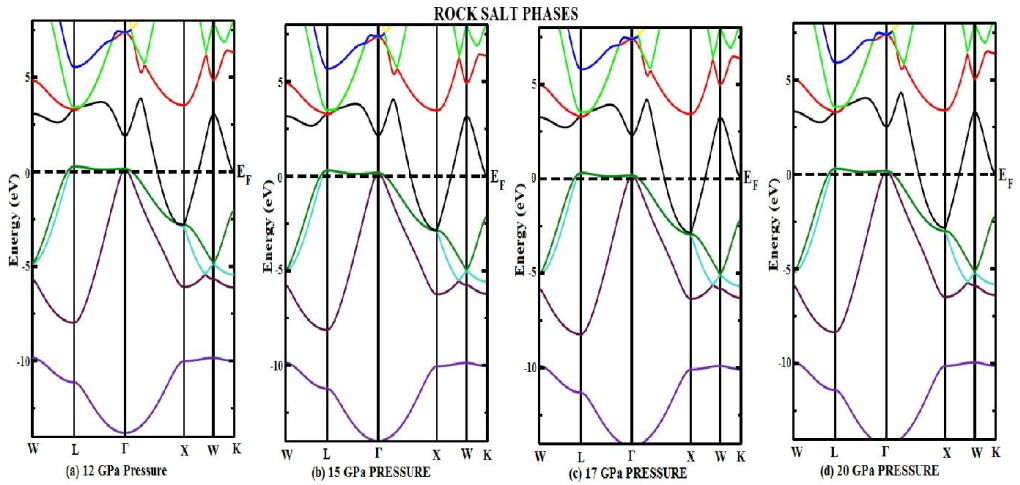

Figure 4.38. Energy band diagram GaAs-RS at (a) 12 GPa pressure (b) 15 GPa pressure (c) 17 GPa pressure and (d) 20 GPa pressure

For GaAs-RS phase, the energy band diagrams of GaAs-RS phase at different pressures are given in figure 4.38(a), (b), (c) and (d). From the figures we find that the metallic nature is retained even at high pressure without much variation.

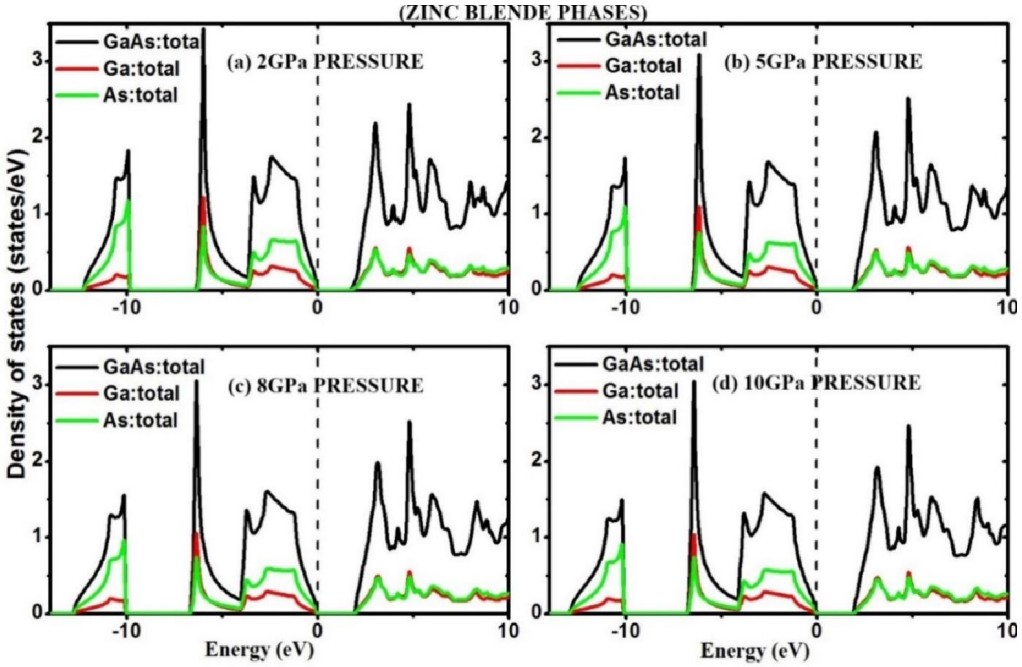

Figure 4.39. Total DOS of GaAs-ZB at (a) 2 GPa pressure (b) 5 GPa pressure (c) 8 GPa pressure and (d) 10 GPa pressure.

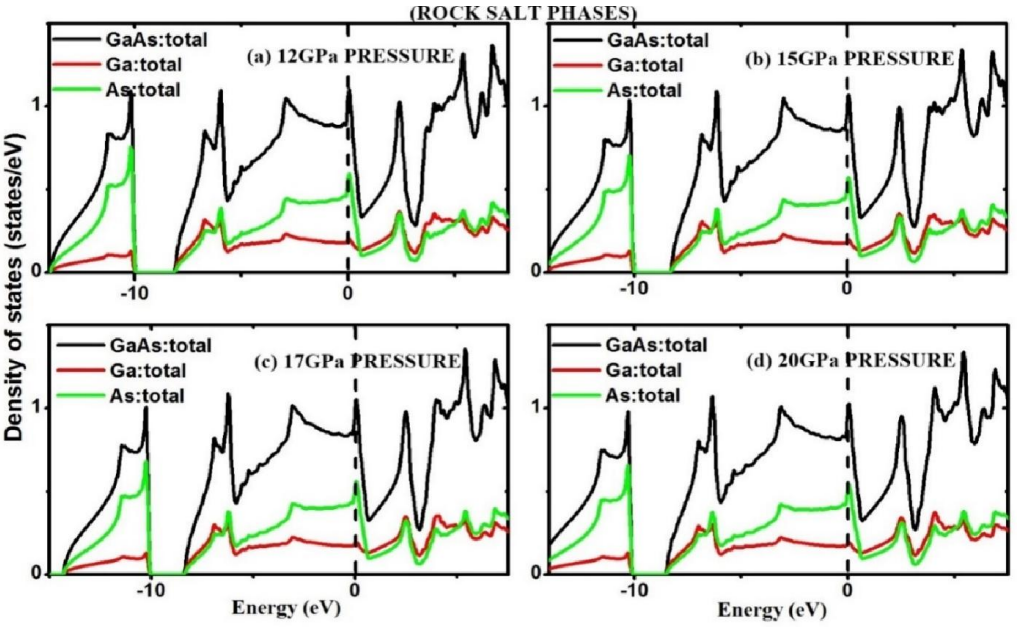

Figure 4.40. Total DOS of GaAs-RS at (a) 12 GPa pressure (b) 15 GPa pressure (c) 17 GPa pressure and (d) 20 GPa pressure.

To further understand the effect of pressure in the band structures, we study the total DOS of GaAs-ZB and GaAs-RS at different pressures. Figure 4.39 shows total DOS of GAaS-ZB at (a) 2 GPa (b) 5 GPa (c) 8 GPa and (d) 10 GPa pressure. In the DOS plot, it is clearly seen the lowest band, valence band and conduction band. The wide of the band between valence band and conduction band give the band gaps under the induced pressure. We also observe a mere variation of this gap under different pressures. This DOS plots support the real understanding of band structure as discussed above (figure 4.36). In figure 4.40, the total DOS of GaAs-RS at (a) 12GPa pressure (b) 15 GPa pressure (c) 17 GPa pressure and (d) 20 GPa pressure are given. In DOS plots, around the Fermi line, crossing over of valence band towards conduction band is clearly observed. Thus the DOS plots confirm the metallic nature as observed in the band diagram (figure 4.38).

4.4.3. Indium Phosphide (InP)

Figure 4.41 and 4.42 show the energy band structure of InP-ZB and InP-RS at zero pressure calculated with (a) LDA, (b) GGA and (c) mBJ-GGA methods. In short, from the band diagrams it concludes that InP-ZB is a direct band gap semiconductor and InP-RS shows metallic nature. As discussed above, the band gap of InP-ZB as obtained with mBJ-GGA is of 1.31eV which is very close to the experimental value of 1.27eV [101].

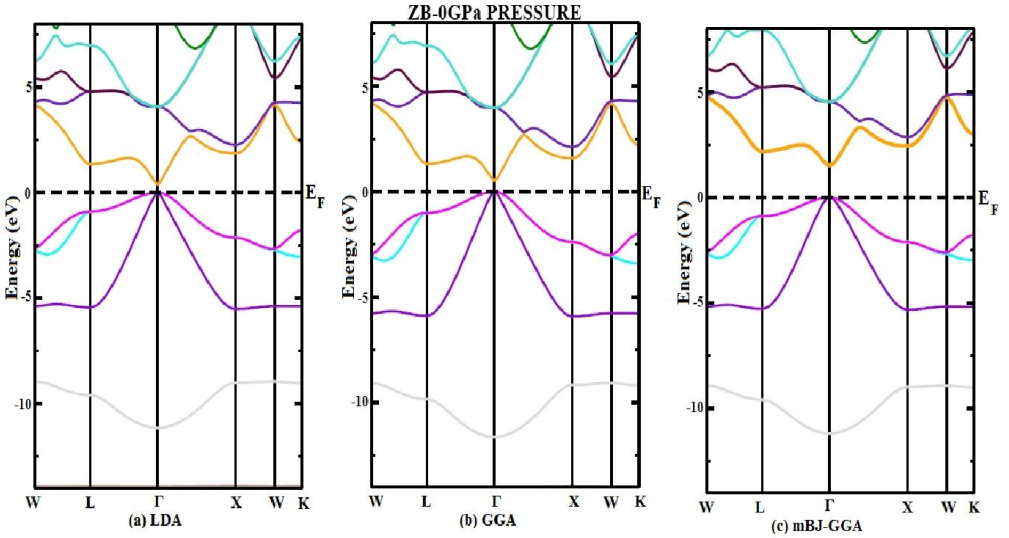

Figure 4.41. Band structure of InP-ZB at 0 GPa pressure within (a) LDA, (b) GGA and (c) mBJ-GGA

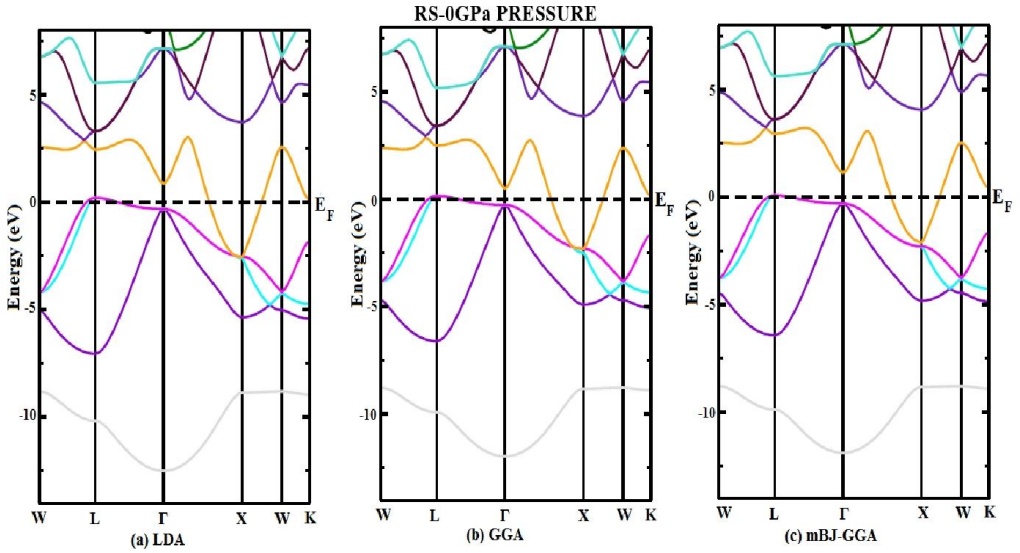

Figure 4.42. Band structure of InP-RS at 0 GPa pressure within (a) LDA, (b) GGA and (c) mBJ-GGA

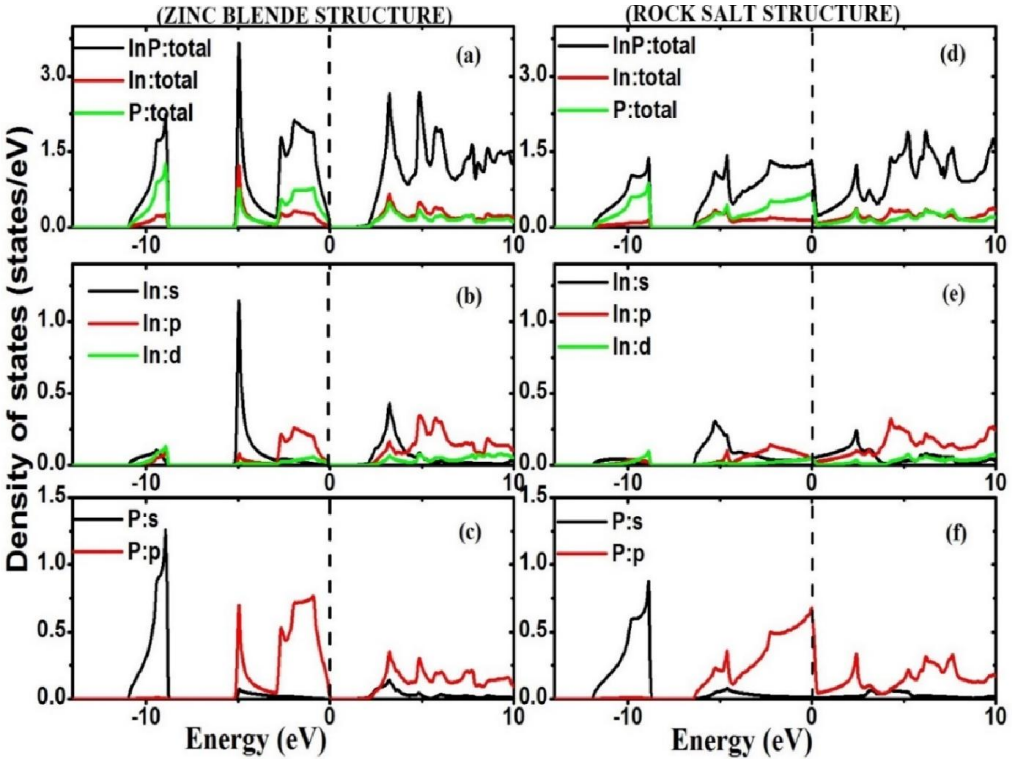

Figure 4.43 Total and Partial DOS of InP-ZB and InP-RS within mBJ-GGA

In figure 4.43 the total and partial DOS of InP-ZB and InP-RS are shown. From figure 4.43(a), (b) and (c) of InP-ZB we observe that the lowest band is mainly contributed by the s-non metal (P atom) orbital with little contribution from the s-metal (In atom) orbital, p-metal (In atom) orbital and d-metal (In atom) orbital and while the valance band is mainly contributed by the s-metal (In atom) orbital with significant contribution from p-metal (In atom) orbital, p-non metal (P atom) and small contribution from p-metal (In atom) orbital and d-metal (In atom) orbital. Again from figure 4.43(d), (e) and (f) for InP-RS we observe that the lowest band is mainly contributed by the s-non metal (P atom) orbital with little contribution from the d-metal (In atom) orbital and s-metal (In atom) orbital while the valance band is mainly contributed by the p-non metal (P atom) orbital along with s-metal (In atom) orbital and s-non metal (P atom) orbital with little contribution from the p-metal (In atom) orbital.

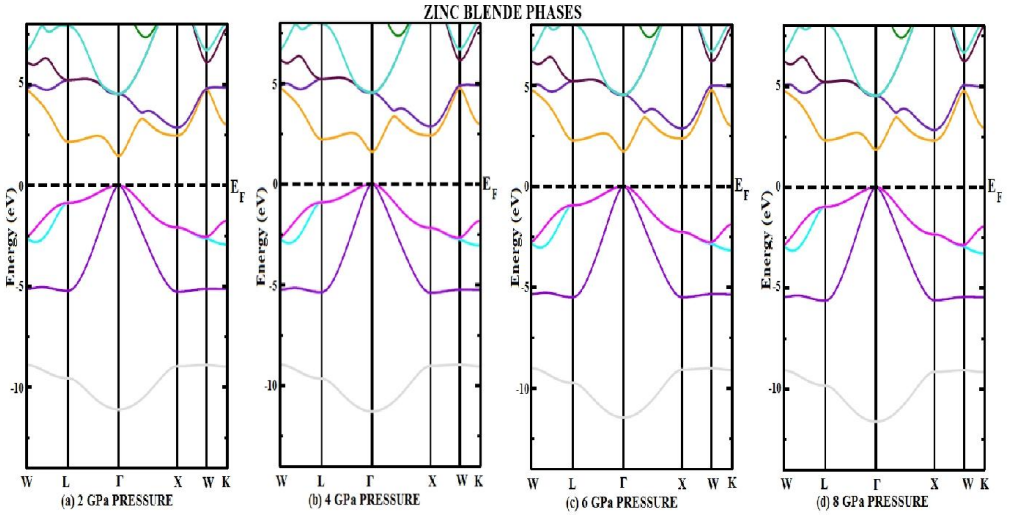

Figure 4.44. Energy band diagram InP-ZB at (a) 2 GPa pressure (b) 4 GPa pressure (c) 6 GPa pressure and (d) 8 GPa pressure

In figure 4.44(a), (b), (c) and (d), the energy band diagrams of InP-ZB phase at different pressures are given. One interesting thing, we see from the band structure diagrams in figure 4.44 is that as the pressure increases to 2 GPa, 4 GPa, 6 GPa and 8 GPa, the gap between the Γ- Γ point increases but if we closely study the energy band diagram we find that the gap at the Γ-L point increases while the gap at the Γ-X point decreases indicating possibility of crossing over at higher pressure. The variation of gap at the Γ- Γ, Γ-L and Γ- X point of InP-ZB with increase in pressure is given in figure 45 for clear analysis.

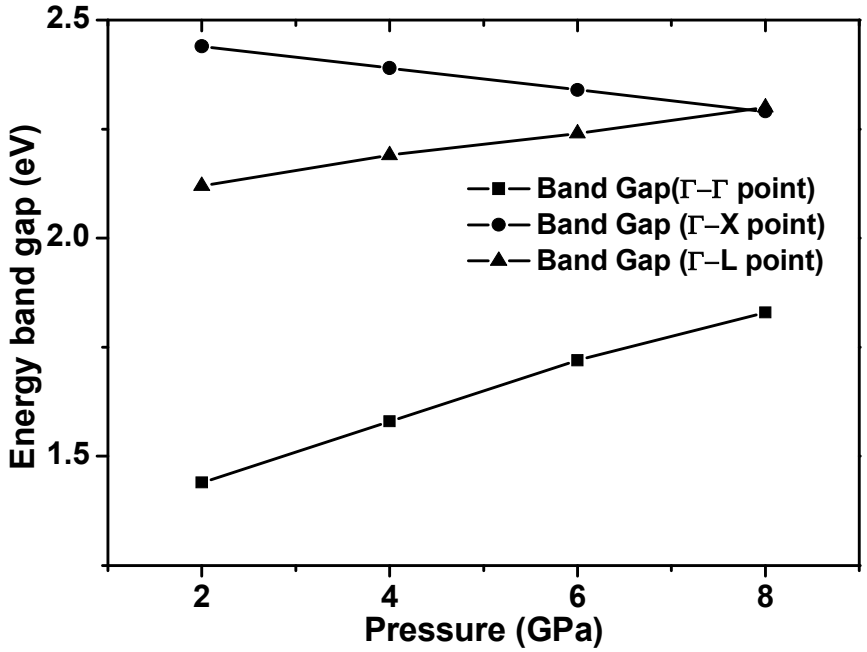

Figure 4.45. Variation of Energy band gaps of InP-ZB phase with pressure

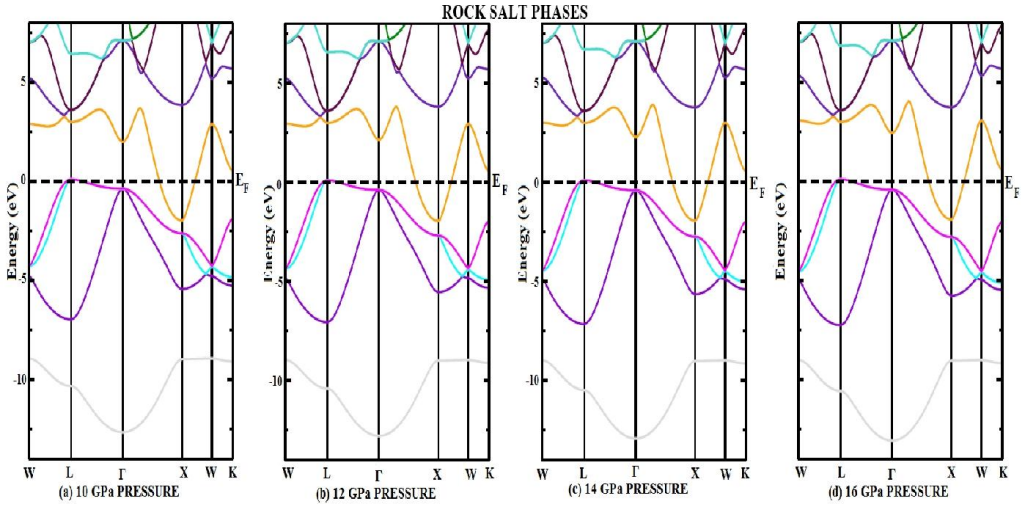

Figure 4.46. Energy band diagram InP-RS in (a) 10 GPa pressure (b) 12 GPa pressure (c) 14 GPa pressure and (d) 16 GPa pressure

In figure 4.46(a), (b), (c) and (d) the energy band diagram of InP-RS phase at different pressures are given. From the figures, we can see that the metallic nature is retained even at high pressure without much variation. Hence we conclude that

the energy band gap of InP-ZB phase is affected by pressure while the energy band gaps of InP-RS phase is not much affected by pressure.

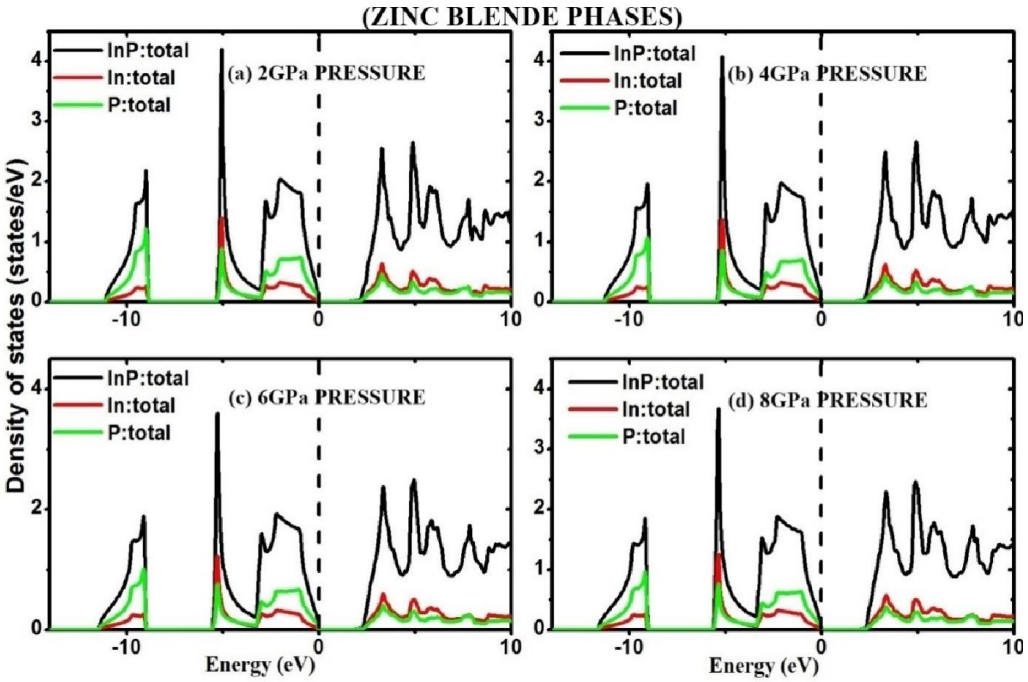

Figure 4.47. Total DOS of InP-ZB at (a) 2 GPa pressure (b) 4 GPa pressure (c) 6 GPa pressure and (d) 8 GPa pressure

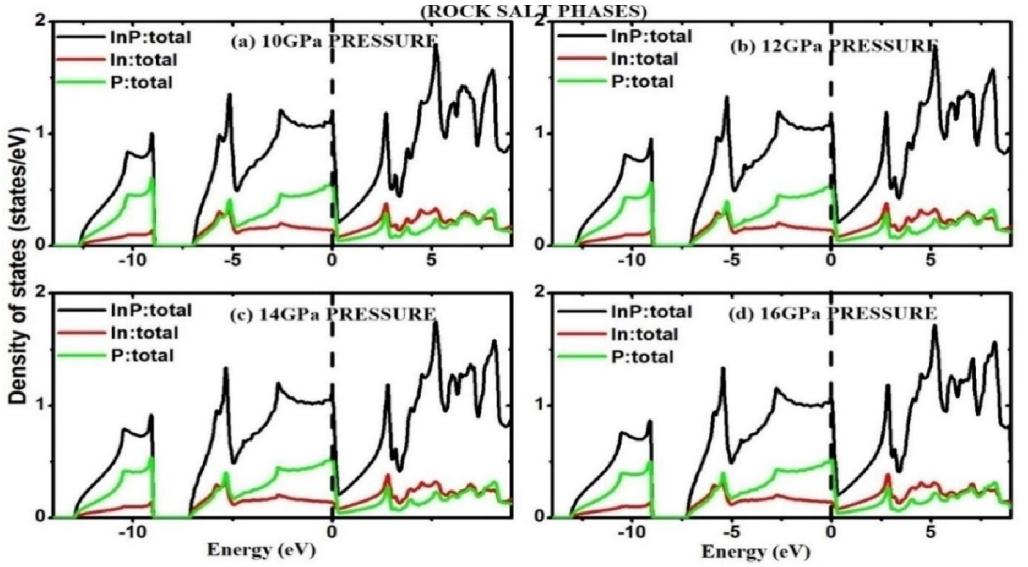

Figure 4.48. Total DOS of InP-RS at (a) 10 GPa pressure (b) 12 GPa pressure (c) 14 GPa pressure and (d) 16 GPa pressure

To further understand the effect of pressure in the band structures we also study the total DOS of InP-ZB and InP-RS at different pressures. In figure 4.47 the total DOS of InP-ZB at (a) 2 GPa pressure (b) 4 GPa pressure (c) 6 GPa pressure and (d) 8 GPa pressure are shown. From the figures, the increase of band gap under induced pressure (as observed in band diagrams in figure 4.44a-d)) is clearly observed in the DOS plots as separation of valence band and conduction band near Fermi line marked on the X-axis. Further, DOS plots of InP-RS as given in figure 4.48 at (a) 10 GPa (b) 12 GPa (c) 14 GPa and (d) 16 GPa pressure show crossing over of valence and conduction band towards Fermi line confirming the metallic nature as concluded before in the band diagrams of figure 4.46.

4.4.4. Indium Arsenide (InAs)

In the above, we have discussed electronic structure of Group III-Vcompound semiconductors in detailed with interpretation. Generally, we observed common characteristics of direct band gap in zincblende structure and metallic nature in rocksalt structure. In short, we have discussed here the electronic structure of InAs. The band structure of InAs-ZB and InAs-RS at zero pressure are shown in figure 4.49 and figure 4.50 respectively. As seen in Figure 4.49 (c) of InAs-ZB with mBJ-GGA, we see a direct band gap of 0.35 eV which is in good agreement to the experimental value of 0.36eV [101] in comparison to LDA, GGA methods. Also figure 4.50 (a-c) of InAs-RS shows metallic nature as indicated due to crossing over of valence and conduction band.

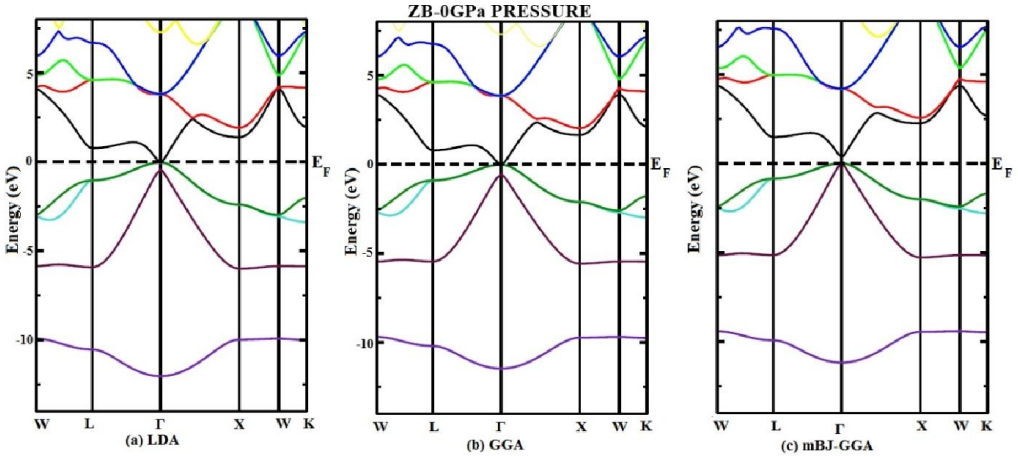

Figure 4.49. Band structure of InAs-ZB at 0 GPa pressure within (a) LDA, (b) GGA and (c) mBJ-GGA

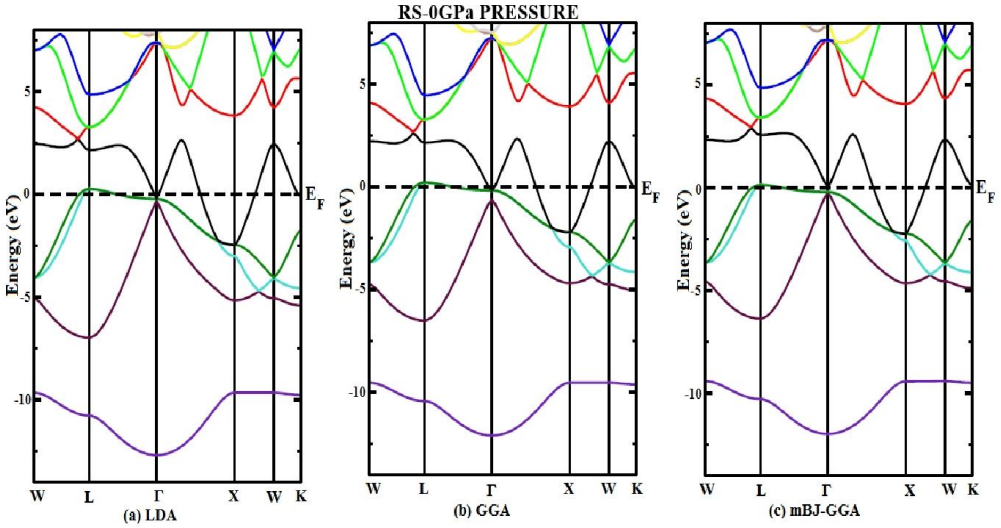

Figure 4.50. Band structures of InAs-RS at 0 GPa pressure within (a) LDA, (b) GGA and (c) mBJ-GGA

In figure 4.51, the total and partial DOS of InAs-ZB and InAs-RS are shown. From figure 4.51(a, b, c), of InAs-ZB, we find that the lowest band is mainly contributed by the As-s state and valance band is contributed by the In-s state with significant contribution from the As-p state and In-p state with little contribution from In-d state. A strong hybridisation is found to occur between the In and As atoms. Again figure 4.51(d, e, f) of InAs-RS, the lowest band is mainly dominated by the As-s state and the valance band is dominated by As-p orbital and In-p orbital.

The band structures of InAs-ZB at 1 GPa, 2 GPa, 3 GPa and 4 GPa pressure are shown in figure 4.52(a, b, c, d). If we closely study the energy band diagrams, it can be observed that the gap at the Γ-L point increases while the gap at the Γ-X point decreases indicating possibility of crossing over at higher pressure. The variation of gap at the Γ- Γ point, Γ-L point and Γ- X point with increase in pressure is given in figure 4.53 for further clear analysis.

In figure 4.54(a, b, c, d) show the energy band diagram of InAs-RS phase at (a) 5 GPa (b) 6 GPa (c) 7 GPa and (d) 9 GPa pressure. Figures show the metallic nature is retained even at high pressure without much variation.

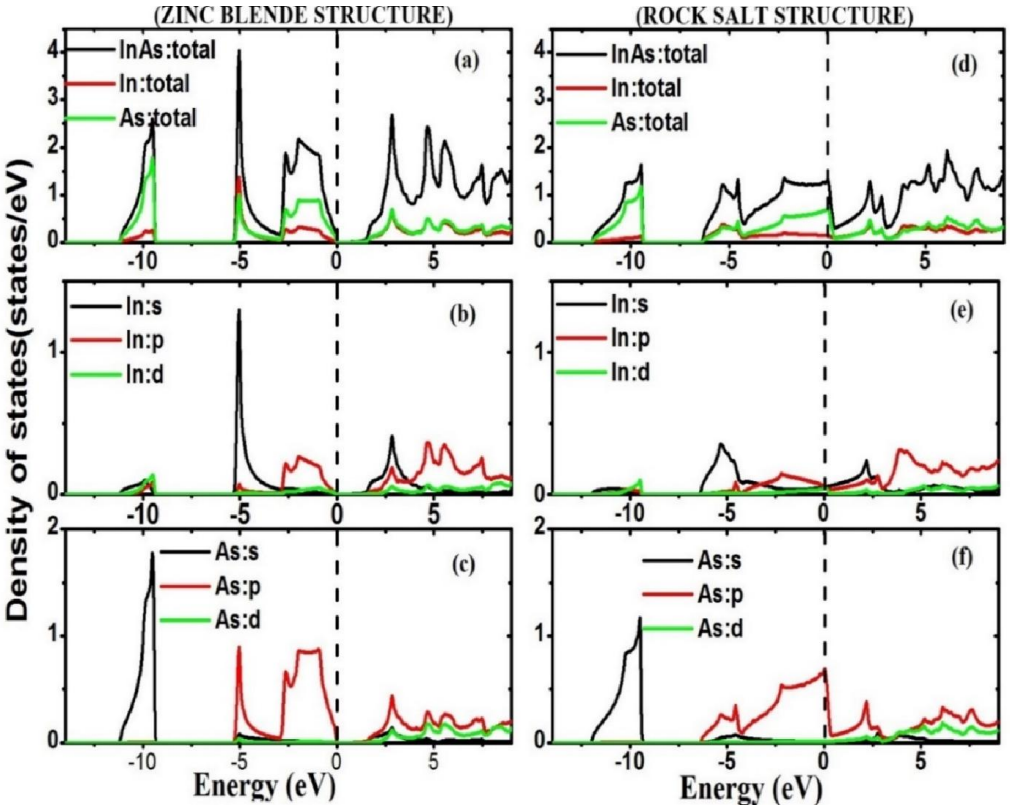

Figure 4.51. Total and Partial DOS of InAs-ZB and InAs-RS within mBJ-GGA

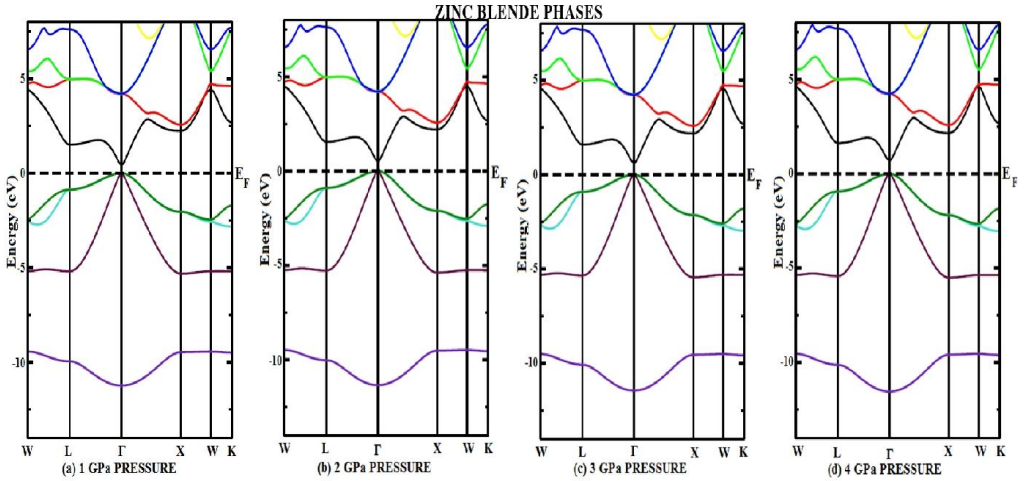

Figure 4.52. Energy band diagram InAs-ZB in (a) 1 GPa pressure (b) 2 GPa pressure (c) 3 GPa pressure and (d) 4 GPa pressure

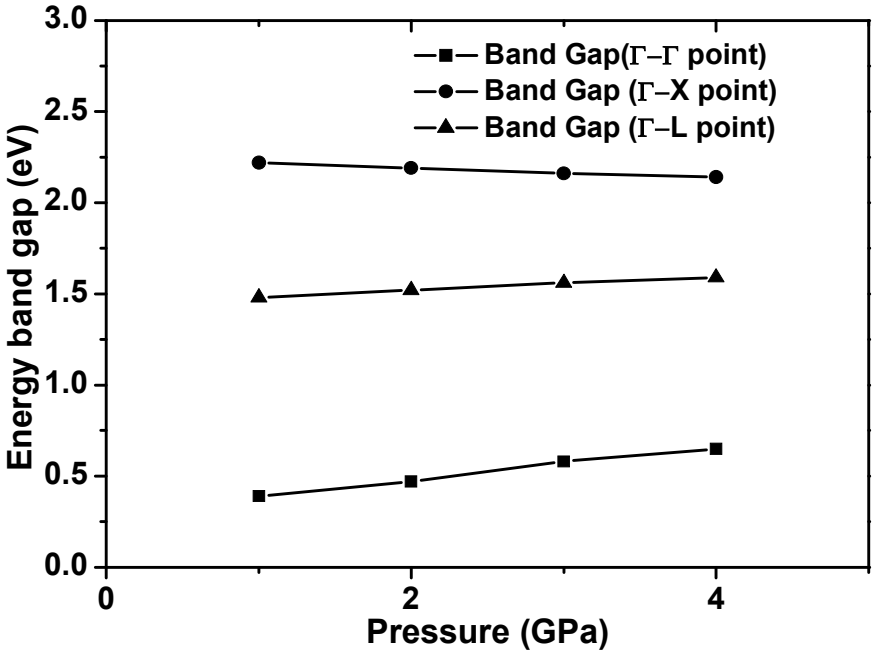

Figure 4.53. Variation of Energy band gaps of InAs-ZB phase with pressure

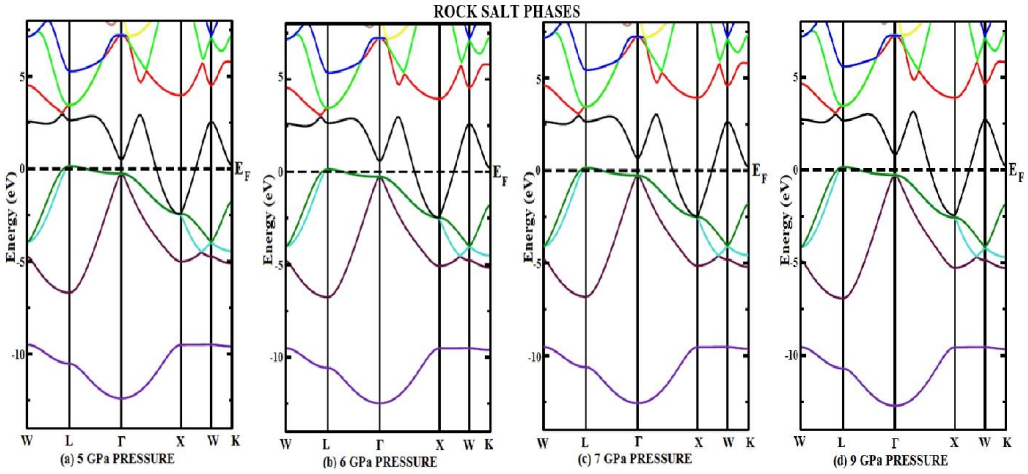

Figure 4.54. Energy band diagram InAs-RS at (a) 5 GPa pressure (b) 6 GPa pressure (c) 7 GPa pressure and (d) 9 GPa pressure

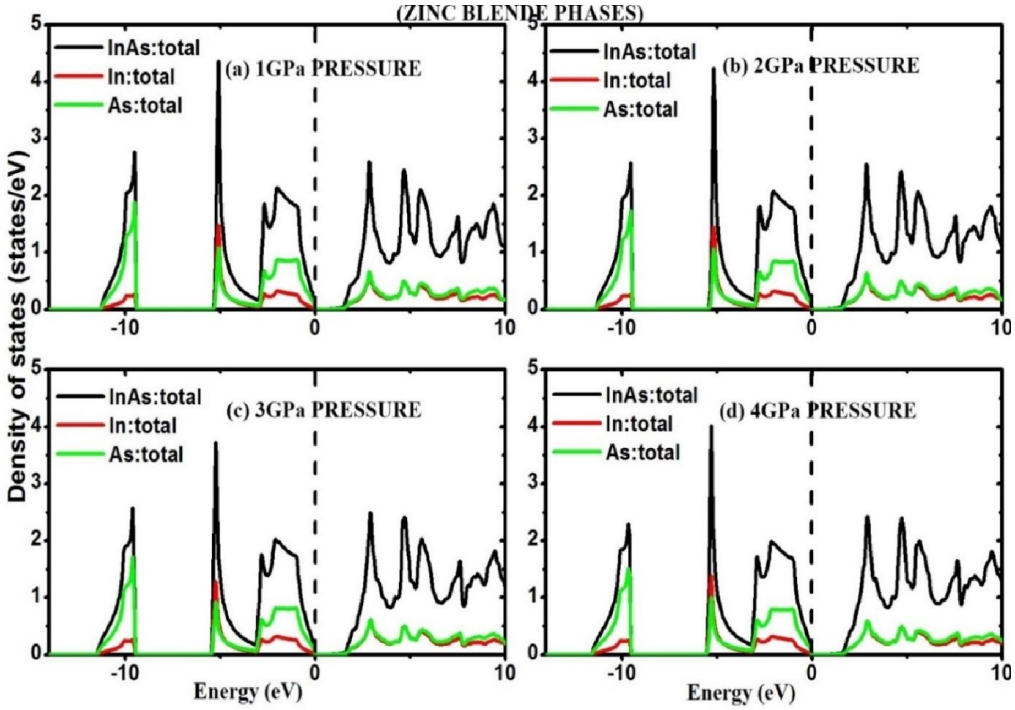

Figure 4.55. Total DOS of InAs-ZB at (a) 1 GPa pressure (b) 2 GPa pressure (c) 3 GPa pressure and (d) 4 GPa pressure

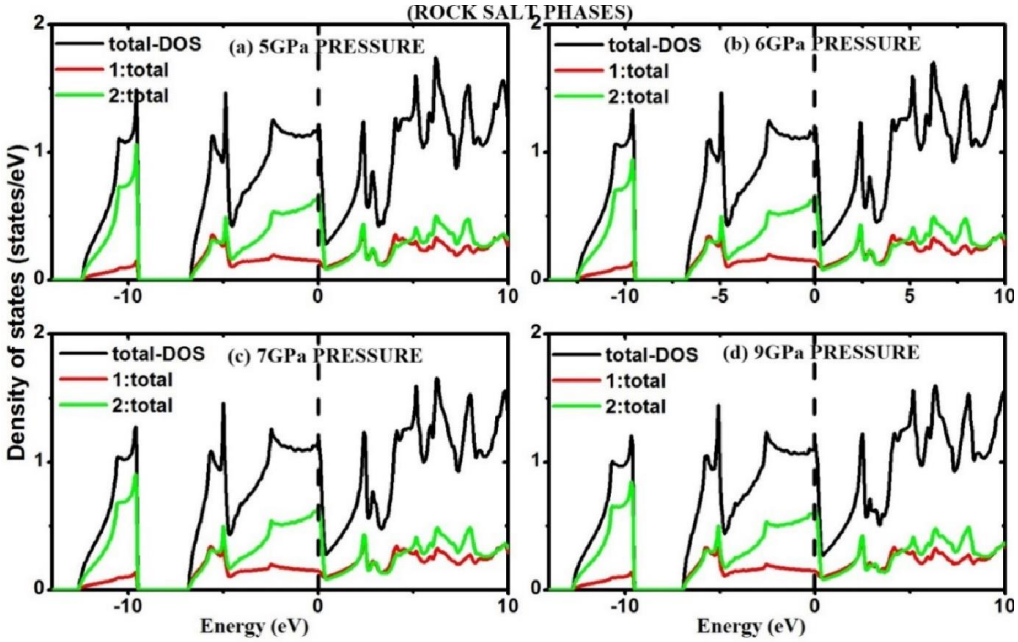

Figure 4.56. Total DOS of InAs-RS at (a) 5 GPa pressure (b) 6 GPa pressure (c) 7 GPa pressure and (d) 9 GPa pressure

In figure 4.55 show the total DOS of InAs-ZB at (a) 1 GPa pressure (b) 2 GPa pressure (c) 3 GPa pressure and (d) 4 GPa pressure. As concluded in the above discussion, the increase of band gap (of InAs-ZB) with increase of pressure is clearly confirmed as the wide of gap between valence band and conduction band around Fermi line in the DOS plots at different pressures (figure 4.55). Figure 4.56(a-e) shows the DOS plots of InAs-RS at 5 GPa 6 GPa, 7 GPa, 9 GPa pressure. Also, the metallic nature of InAs-RS as oberved in the band diagrams (in figure 4.54) is clearly confirmed in the DOS plots (figure 4.55) as crossing over of valence and conduction band around Fermi line.

4.5. CONCLUSION

The structural properties of group III-V compound semiconductors such as GaP, GaAs, InP and InAs in both zincblende (ZB) and rocksalt (RS) are studied and found to be in good agreement with the experimental and theoretical results. The structural phase transformation from the ZB to RS structure under induced pressure

has also been performed for these compounds and the volume collapse at the transition pressure determined.

i. The structural parameters of GaP, GaAs, InP and InAs are calculated with both the LDA and GGA methods as given in table 4.1, table 4.4, table 4.7 and table 4.10.

ii. The structural phase transition from the ZB to RS of

- GaP are found to occur at 21.9 GPa pressure with a volume collapse of 14.11% at the transition pressure
- GaAs at 10.7 GPa pressure with a volume collapse of 14.2% at the transition pressure,
- InP at 9.3 GPa pressure with a volume collapse of 16.45% at the transition pressure,and
- InAs at 4.7 GPa pressure for InAs with a volume collapse of 17.2% at the transition pressure,

iii. The elastic constants (C_{11}, C_{12} and C_{44}) of both the ZB nad RS phases are found to satisfy the mechanical stability conditions and undergo a linear variation with increase in pressure. The elastic parameters (Zener Anisotropy factor (A), Poisson's ratio (υ), Kleinmann parameter (ζ), B/G ratio, Young's modulus (Y) and Deby's temperature (θ_D)) are also calculated.

iv. The energy band gaps of the ZB and RS structures at zero pressure of GaP, GaAs, InP and InAs are calculated using the LDA, GGA and mBJ-GGA potentials. The implementation of the mBJ-GGA potential in the energy band gap calculation resolves the underestimation of the band gaps with

LDA, GGA and provides better results closer to the experimental value. In the energy band diagram it is observed that

- GaP is an indirect band gap semiconductor and energy band gap calculated with mBJ-GGA method is of 2.33eV.
- GaAs, is a direct band gap semiconductor within mBJ-GGA method with a gap of 1.3eV.
- InP is a also direct band gap semiconductor of 1.31eV within mBJ-GGA method.
- Lastly in case of InAs, calculation of the energy band structure within the mBJ-GGA method shows a direct band gap of 0.35 eV

v. The corresponding total and partial DOS for the ZB and RS structures at zero pressure are studied within the mBJ-GGA method only. The energy band structures as well as the DOS for both ZB and RS structures are studied at different pressures. For all the four compounds (GaP, GaAs, InP and InAs) in ZB phase, as the pressure increases the energy band gap between the Γ-L increases but the gap between Γ-X are found to decrease towards the fermi level indicating possibilities of crossing over of the conduction band towards the valance band and confirming the metallic nature of the RS phases of these compounds at higher pressure. But in the RS phases of these compounds (GaP, GaAs, InP and InAs) the metallic nature is retained even at high pressure without much variation. Hence we conclude that the energy band gap of ZB phases of GaP, GaAs, InP and InAs are affected by pressure while the energy band gaps of the RS phases are not much affected by pressure.